A DENDRIMER-BASED PRODRUG FOR USE IN AN ANTI-CANCER NANOCELL

by

Samir Awasthi

S.B., Physics
Massachusetts Institute of Technology (2006)

Submitted to the Department of Biological Engineering
In Partial Fulfillment of the Requirements for the Degree of

MASTER OF ENGINEERING IN BIOMEDICAL ENGINEERING

at the

MASSACHUSETTS INSTITUTE OF TECHNOLOGY

MAY 2007
[June 2007]

Signature of Author: _____
Department of Biological Engineering
May 11, 2007

Certified by: _____
Ram Sasisekharan
Professor of Biological Engineering and Health Sciences and Technology
Thesis Supervisor

Certified by: _____
Shiladitya Sengupta
Assistant Professor of Medicine and Health Sciences and Technology
Thesis Supervisor

Accepted by: _____
Bevin P. Engelward
Associate Professor of Biological Engineering
Chair, Department of Biological Engineering Graduate Committee

A DENDRIMER-BASED PRODRUG FOR USE IN AN ANTI-CANCER NANOCELL

by

Samir Awasthi

Submitted to the
Department of Biological Engineering

May 11, 2007

In Partial Fulfillment of the Requirements for the Degree of
Master of Engineering in Biological Engineering

Abstract

Cancer science is a heavily researched and rapidly changing field. Cutting edge research consistently reveals unique features of tumors that can be exploited for treatment. For example, it is well known that cells of varying tumor types have unique molecular markers and cell-surface receptors – fingerprints of sorts – that set cancerous cells apart from healthy cells. Furthermore, the tumor microenvironment has been explored to the point that its unique fluid mechanical and biochemical properties are well understood in the context of tumor growth and survival. However, very little of this research has penetrated clinical medicine. The purpose of this thesis is to present a recent concept in cancer therapy: an anti-cancer nanocell that is capable of the spatial and temporal targeting of drugs to tumor cells. The combination of targeting mechanisms designed into the nanocell is a product of our current understanding of tumors. The design serves to improve the effectiveness of inexpensive, out-of-patent cytotoxic and anti-angiogenic drugs to standards representative of modern research. Efforts towards improving the efficiency of the nanocell, with regards to both drug loading and tumor cell targeting, are presented and discussed. The synthesis of various polymer-ligand conjugates for use in the improved nanocell is reported, as is the development of a prodrug consisting of a generation three polyamidoamine dendrimer conjugated to methotrexate via an ester bond; cell studies demonstrating the effectiveness of the prodrug are included. The expandability of the nanocell is also explored, because ultimately, the nanocell must be robust enough to accommodate both tumor-type and population variability.

Thesis supervisor: Ram Sasisekharan
Title: Professor of Biological Engineering and Health Sciences and Technology

Thesis supervisor: Shiladitya Sengupta
Title: Assistant Professor of Medicine and Health Sciences and Technology

Acknowledgements

The work presented in the following thesis was performed in the laboratories of Professors Ram Sasisekharan and Shiladitya Sengupta, of the Department of Biological Engineering at the Massachusetts Institute of Technology, and the Harvard-MIT Division of Health Sciences and Technology, respectively.

First and foremost, I would like to thank my co-supervisors, Dr. Ram Sasisekharan of the Department of Biological Engineering at MIT, and Dr. Shiladitya Sengupta of HST, for giving me the opportunity to join such an exciting and innovative research project. It is in no small part due to their guidance and supervision that this work was completed successfully. I would also like to thank Dr. Geeti Gangal, a postdoctoral associate in the Sengupta laboratory. I worked very closely with Dr. Gangal throughout the project, and her unparalleled guidance and instruction was an essential aspect of the work. I owe much of my knowledge of the chemistry behind the nanocell to Geeti. In addition to Dr. Gangal, I would also like to thank Dr. Pochi Shum and Dr. Sujan R. Kabir, also of the Sengupta Laboratory. They both contributed indispensably to the work presented here, and also to my knowledge of the science underlying the project – this thesis is a direct result of a whole group's effort towards one goal.

Finally, I would like to thank my family for supporting me, not only throughout my time at MIT, but also throughout my entire life. I owe every opportunity that I have had to my family. Without wisdom and support from my parents, and advice and guidance from my siblings, I would not be where I am today.

Contents

List of Figures

Chapter 1

Introduction

1.1 Background

Cancer is a leading cause of death in the United States; it accounts for 23% of all deaths in the nation. The lifetime probability of getting cancer is nearly 50% for men and 33% for women. For children, the probability of getting cancer between the ages of zero and fourteen is 15%. While the mortality of the disease varies significantly depending on the type of cancer, the time of diagnosis, and patient demographic, the treatments currently available for all types of cancers are fairly unsophisticated. They are not wholly specific for cancer tissue microenvironments and they, in general, do not have spectacular cure rates. Furthermore, cancer survival rates have not improved appreciably in the past 50 years (all statistics from The American Cancer Society, 2004). As cancer awareness rises and diagnostic methods improve, the need to develop more effective treatments for cancer is ever more emphasized.

Currently, there exist several different options for cancer treatment, and most cancer patients undergo some combination of the available therapies.

1.1.1 Current Treatment Options

Surgery: surgery is a procedure performed on nearly all cancer patients as a diagnostic procedure. It is also used as a treatment; when it is, it is usually accompanied by radiation therapy, chemotherapy, and/or anti-angiogenesis therapy. The objective of a surgical anti-cancer intervention is to remove as much of the primary tumor as possible, and then allow ionizing radiation or chemotherpeutic agents to kill the remaining tumor cells. The primary drawback of surgery is that it is invasive, it may result in physical abnormalites, and it also involves the side-effects of therapies that it is combined with. Furthermore, a surgical intervention targets primary tumors only; smaller metastases are generally not treated by surgery. In fact, research has shown that the surgical resection of a primary tumor can spark the growth of dormant metastatic tumors, due to the loss of endogenous angiogenesis inhibitors produced by the primary tumor [O'Riley et al., 1994].

Radiation Therapy: radiation therapy is a very common form of treatment in which tumors are targeted and irradiated by a source of ionizing radiation; approximately half of all cancer patients receive some form of the treatment. It was thought that the primary action of radiation therapy is to cause mutations in the DNA of irradiated cells, and thereby induce apoptosis during the replication phase of those cells' lives. However, recent research suggests that the apoptotic effects of ionizing radiation arise from intercellular signals that originate from irradiated endothelial cells [Gorsky et al. 1999].

Generally, radiotherapy is administered externally via an IR producing machine, or internally via implanted sources of IR, depending on the type of tumor being treated.

Radiation therapy is most often used to treat primary tumors. One benefit of radiation therapy over surgical resection is that the pro-metastatic effect of the surgical treatment of primary tumors is not observed following radiation therapy [Hartfor et al., 2000]. However, a significant disadvantage of radiation therapy is that it damages the normal tissue surrounding the tumor. As such, there is a strong research push to develop tumor-targeted radiosensitizers, normal tissue-radioprotectors, and the technology to precisely shape radiation pulses such that they are absorbed in a preselected region.

Chemotherapy: chemotherapy is the administration of cytotoxic drugs that target and cause lethal damage to cells undergoing mitosis. Because cancer cells are dividing much more rapidly than most other cells in the body, chemotherapeutic drugs are particularly effective against tumors. However, these drugs can also affect normal, rapidly dividing cells, including bone marrow cells and cells of the gastrointestinal tract. Thus, determining the correct dosage is very important, and will depend on both the tumor and the patient.

Other: more modern anti-cancer therapies also exist, though most of them are in clinical trials, or being researched heavily. These therapies include anti-angiogenesis therapy, immunotherapy, photodynamic therapy (PDT), and most recently, pharmaceuticals that target important signaling pathways in specifc tumor cell types. Of these options, anti-angiogenesis therapy has received the most attention, as it has shown significant promise when combined with radiotherapy and chemotherapy. The first anti-angiogenesis drug, Avastin (bevacizumab) has already been approved for use with chemotherapeutic agents.

Combination Therapies: combination therapies are among the most effective and widely used forms of cancer treatment available. Physicians implement such therapies by strategically combining multiple treatment modalities in order to eliminate a given tumor. Nearly all cancer patients today receive some form of multi-modal therapy. The combination of surgery and radiation therapy was already mentioned above, but chemotherapy is also often used in conjunction with radiation therapy and/or surgery.

Combination approaches involving chemotherapy are of particular interest, because of their widespread use. In the case of chemotherapy alone, cytotoxic drugs are not as effective in the center of a tumor as they are on the tumor periphery. The decline in effectiveness is due in part to abnormalities in the vasculature and interstitial environments of tumors; such abnormalities prevent chemotherapeutic agents from readily diffusing to the center of the tumor [Jain 1997]. However, it is also due to the fact that cells at the center of a tumor do not divide as rapidly as cells at the periphery (cytotoxic drugs target rapidly dividing cells). Thus, to effectively eliminate a tumor, chemotherapy is often combined with different treatment modalities; its combination with anti-angiogenesis therapy shows significant promise.

1.1.2 The Synergy of Chemotherapy and Anti-Angiogenic Agents

Cancer treatment is a heavily researched and rapidly changing field. In the clinic, the combination of multiple treatment modalities is becoming the favored approach. Of the various strategies used, the combination of chemotherapy and anti-angiogenesis therapy is promising due to its effectiveness and lack of additional toxicity [Klement et

al.]. However, certain challenges must be overcome before the combination treatment is maximally effective.

In considering the combination of chemotherapy with anti-angiogenesis therapy, it is important to consider a relatively new concept in cancer biology: the normalization of a tumor's vasculature in response to anti-angiogenic drugs. For some time, the conventional belief regarding anti-angiogenesis therapy held that the administration of angiogenesis inhibitors resulted in the destruction of a tumor's vasculature, and little more. Consequently, anti-angiogenesis therapy would starve a tumor to of oxygen and nutrients, and inhibit its growth and survival. However, recent research suggests that, in the course of destroying tumor vasculature, certain anti-angiogenic agents can actually cause the vasculature to become more "normal" and efficient at delivering nutrients for a brief period of time [Jain 2005]. In brain tumors, this was shown to happen through increased pericyte coverage and a corresponding activation of matrix metalloproteinases [Winkler et al. 2004]. The transient normalization provided by antiangiogenic agents can alleviate the hypoxic, high fluid pressure microenvironments of tumors and also allow for improved drug delivery to the tumor interior. It has become increasingly apparent that the window of normalization provided by anti-angiogenesis agents, such as VEGFR-2 antibody and thalidomide, can be used to optimize the response of tumors to cytotoxic therapies [Tong et al. 2004, Ansiaux et al. 2005].

After the transient phase of vascular normalization, the tumor becomes more hypoxic, and various stress-response mechanisms are activated. In particular, hypoxia induces the accumulation and activation of hypoxia-inducible factor-1α (HIF-1α) [Carameliet et al. 1998]. HIF-1α accumulation and activation is known to increase

tumor cell chemotherapy resistance [Semenza et al. 2000]. Also, as expected, the regression of the tumor vasculature beyond the normalized state results in a decrease in the effectiveness of the blood-based delivery of substances to the center of the tumor.

Two major problems exist in the combination of chemotherapy with anti-angiogenesis therapy. First, because the therapies are not administered in a time-controlled manner, such that the cytotoxic drug is delivered while the tumor vasculature is in a normalized state, the effectiveness of chemotherapy is reduced both by diffusion limitations and by the HIF-1α mediated stress-response mechanism discussed above. Second, because neither cytotoxic drugs nor anti-angiogenic drugs are presently targeted to tumor cells, the combination therapy acts on any rapidly dividing cell or developing vascular network (germ cells, bone marrow cells, hair follicles, etc.). The side-effects due to such indiscriminate drug delivery can be painful and debilitating.

However, if the two therapies are strategically administered, the combination treatment can be beneficially synergistic. In an ideal situation, the cytotoxic and anti-angiogenic drugs would be delivered specifically to tumor microenvironments, and the delivery would occur during phases of vascular normalization. The typical side-effects of indiscriminate intravenous treatment would be avoided, while higher intratumoral concentrations of the administered drugs could be achieved. To attain this synergy with the current arsenal of FDA-approved anti-cancer drugs, a novel way of spatially and temporally targeting anti-cancer drugs is required.

Spatial tumor targeting can be achieved by taking advantage of the increased porosity of tumor vasculature. By designing a delivery vehicle that can pass through the large pores in tumor blood vessels, but not through the smaller pores of normal vessels, a

fair amount of spatial tumor targeting can be achieved [Hobbs et al. 1998, Yuan et al. 1995]. Furthermore, such targeting can be enhanced by the use of ligands that target specific cell-surface receptors that are over expressed on tumor cells. Folic acid is one such ligand [Hilgenbrink and Low, 2005], because it is involved in DNA synthesis, and its cell-surface receptor over-expressed on many rapidly dividing cells.

Temporal targeting can be achieved through careful design of the delivery vehicle. The vehicle would need to be capable of delivering both the anti-angiogenesis and chemotherapy drugs at the same time, but then releasing them sequentially (anti-angiogenesis drug first) in order to isolate the chemotherapeutic agent within the tumor. The timescale of the process would have to allow anti-angiogenesis therapy to complete before the cytotoxic drug takes effect, thereby trapping the cytotoxic drug in the tumor at high concentrations.

1.2 Previous Work

A novel drug delivery vehicle that meets the criterion discussed above, termed the "nanocell," has been developed in the Sasisekharan laboratory at MIT [Sengupta et al. 2005]. The nanocell is designed such that it delivers both cytotoxic and anti-angiogenic drugs to tumors in the spatially and temporally targeted manner. The core of the nanocell a nanoparticle that is composed of doxorubicin, a DNA-intercalating cytotoxic drug, conjugated to the copolymer poly-(lactic-co-glycolic) acid (PLGA). A phospholipid block-copolymer envelope encapsulates the inner nanoparticle, an anti-angiogenesis drug

is held in between the nanoparticle and envelope. The anti-angiogenesis drug is combretastatin A-4 phosphate, a biomolecule that disrupts vascular networks by inducing tubulin depolymerization in endothelial cells. Upon synthesis, the nanocells range from 180-200 nanometers in diameter.

The design of the nanocell allows both spatial and temporal tumor targeting to be achieved. Spatial tumor targeting is primarily a result of the size of the nanocell. Compared to normal vasculature, the vasculature of growing tumors is known to be very porous, with pore diameters ranging from 200 to 600 nanometers depending on tumor type [Yuan et al., 1995]. Because normal vessel pores are much smaller, the 180 - 200 nanometer nanocell selectively diffuses into tumors from the bloodstream. Upon entering a tumor, the nanocell envelope destabilizes, and both the free-floating anti-angiogenesis drug and nuclear nanoparticle are released. The anti-angiogenesis drug acts immediately, destabilizing the tumor vasculature as the treatment with the nanocell continues. During the course of treatment, the tumor vasculature is normalized, and more and more nanocells accumulate in the tumor; by the time the vasculature has been destroyed, high intratumoral concentrations of the nuclear nanoparticles have been achieved. In time, the nanoparticles slowly release the bound cytotoxic drug, and the combination therapy is successfully completed.

Experiments on mice with tumor xenografts demonstrated that treatment with the nanocells does indeed have the intended effects. Relative to control treatments, treatment with the nanocell decreased HIF-1α presence in tumors and also increased tumor cell apoptosis rates. Furthermore, treatment with the nanocell resulted in a greater than additive increase in mouse lifespan over the various control groups. The results were

published by Sengupta et al. in 2005. The work represented the proof-of-concept necessary to take the nanocell to industry.

Despite the success of the nanocell as designed, it was clear that certain aspects of it needed to be improved before it could translate into a clinical setting. In particular, there was an unmet need to develop a more efficient tumor cell targeting process and to the loading mechanism of the nanocell.

1.3 Thesis Work

The bulk of this thesis describes the synthesis work and design principles involved in meeting the needs described above. Three primary projects were undertaken:

1. To attempt to remake the nanocell envelope using chitosan, instead of using the polyethylene glycol-disteroyl phosphatidylethanolamine (PEG-DSPE) liposome from the original study.

2. To incorporate receptor targeting into the envelope of the nanocell, using folate as a proof-of-concept targeting ligand.

3. To design a methotrexate prodrug using the polyamidoamine dendrimer, for encapsulation within the nanocell.

The first project was undertaken to improve the cost-effectiveness of the nanocell. Part of the motivation of the nanocell is that through its multiple layers of tumor

targeting, the therapeutic index of various out-of-patent anti-cancer drugs can be improved dramatically, thereby making cutting edge cancer treatment available to the developing world at a relatively low price. The first project was undertaken to improve the cost-effectiveness of the nanocell. Chitosan is a widely available, established biomaterial that has already been used in several biomedical applications; indeed, it has already been used for the synthesis of nanoparticles and nanospheres [Bodnar et al. 2005]. Furthermore, various ligands can be conjugated to chitosan via its amine side groups. As such, it was viewed as an ideal envelope material. However, the use of chitosan proved to be problematic, and due to reason that will be discussed in chapter two, its use in the nanocell was abandoned.

The second project was undertaken to improve the spatial tumor targeting of the nanocell. Tumor cells of varying type are known to overexpress certain cell-surface molecular receptors. For example, ErbB, HER-2/neu, EGFR, and the folate receptor are known to be overexpressed varying types of tumors [Richter and Zhang, 2005]. Accordingly, we decided to incorporate receptor targeting into the envelope of the nanocell in order to introduce an additional layer of tumor cell targeting beyond selective diffusion. As proof-of-concept, folic acid was used as the targeting ligand, because it is a common and readily obtainable molecule. More importantly, and ligand that can be conjugated to an amine or hydroxyl functional group may be used as a targeting ligand in the redesigned nanocell.

The third and most substantial project undertaken was the design of a methotrexate prodrug that would improve the loading efficiency of the nanocell while also introducing another layer of tumor-environment targeting. In order to create a

consistently sized, highly loaded prodrug, a polyamidoamine dendrimer was used as the core of the prodrug. The dendrimer was of the third generation, and contained thirty-two hydroxyl surface-functional groups. Through these functional groups, methotrexate was conjugated to the dendrimer via an ester bond. The ester linkage was chosen because abundant cellular esterases would cleave the cytotoxic drug from the dendrimer. The consistent size of the dendrimer (see chapter two), and its biological activity (see chapter three), both corresponded to the goals.

Together, the work presented in the following chapters represents the design and synthesis of components that will be used to improve the therapeutic index of the nanocell, thereby moving the nanocell a step towards being used in a clinical setting. With an inexpensive, efficient, biocompatible nanocell, the challenges facing combination therapy can be overcome, and the full benefit of combining multiple cancer treatment modalities can be realized.

Bibliography

American Cancer Society, Inc. "Cancer Statistics 2004." http://www.cancer.org/docroot/pro/content/pro_1_1_Cancer_Statistics_2004_presentation.asp. Copyright 2004.

Ansiaux R, Baudelet C, Jordan B, Beghein N, Sonveaux P, Wever JD, Martinive P, Grégoire V, Feron O, Gallez B. Thalidomide Radiozensitizes Tumors through Early Changes in the Tumor Microenvironment. *Clin Can Res.* **11**: 743-750 (2005).

Bodnar M, Hartmann JF, Borbely J. Preparation and Characterization of Chitosan-Based Nanoparticles. *Biomacromolecules.* **6**:2521-2527 (2005).

Carameliet P, Dor Y, et al. Role of HIF-1a in hypoxia-mediated apoptosis, cell proliferation, and tumour angiogenesis. *Nature.* **394**:485-490 (1998).

Gorsky DH, Beckett MA, Jaskowiak NT, Calvin DP, Mauceri HJ, Salloum RM, Seetharam S, Koons A, Hari DM, Kufe DW, Weichselbaum RR. Blockade of the Vascular Endothelial Growth Factor Stress Response Increases the Antitumor Effects of Ionizing Radiation. *Cancer Research.* **59**:3374-3378 (1999).

Hartford AC, Gohongi T, Fukumura D, Jain RK. Irradiation of a primary tumor, unlike surgical removal, enhances angiogenesis suppression at a distal site: Potential role of host-tumor interaction. *Cancer Research.* **60**:2128-2131 (2000).

Hilgenbrink AR and Low PS. Folate receptor-mediated drug targeting: from therapeutics to diagnostics. *J Pharm Sci.* **94**(10):2135-2146 (2005).

Hobbs SK, Monsky WL, Yuan F et al. Regulation of transport pathways in tumor vessels: role of tumor type and microenvironment. *PNAS.* **95**:4607-4612 (1998).

Jain RK. Delivery of molecular and cellular medicine to solid tumors. *Microcirc.* **4**(1):1-23 (1997).

Jain RK. Normalization of Tumor Vasculature: An Emerging Concept in Antiangiogenic Therapy. *Science.* **307**:58-62 (2005).

Klement G et al. Continuous low-dose therapy with vinblastine and VEGF receptor-2 antibody induces sustained tumor regression without overt toxicity. *J Clin Invest.* **105**:R15-R24.

O'Riley MS, Holmgren L, Shing Y, Chen C, Rosenthal RA, Moses M, Lane WS, Cao Y, Sage EH, Folkman J. Angiostatin: a novel angiogenesis inhibitor that mediates the suppression of metastases by a Lewis lung carcinoma. *Cell.* **79**:315-328 (1994).

Richter M and Zhang H. Receptor-targeted cancer therapy. *DNA Cell Biol.* **24**(5):271-282 (2005).

Semenza GL. Surviving ischemia: adaptive responses mediated by hypoxia-inducible factor 1. *J Clin Invest.* **106**:809-812 (2000).

Sengupta S, Eavaron D, Capila I, Zhao G, Watson N, Kiziltepe T, Sasisekharan R. Temporal targeting of tumour cells and neovasculature with a nanoscale delivery system. *Nature.* **436**:568-572 (2005).

Tong DT, Boucher Y, Kozin SV, Winkler F, Hicklin DJ, Jain RK. Vascular Normalization by Vascular Endothelial Growth Factor Receptor 2 Blockade Induces a Pressure Gradient Across the Vasculature and Improves Drug Penetration in Tumors. *Cancer Research.* **64**:3731-3736 (2004).

Winkler F, Kozin SV, Tong RT, Chae S, Booth MF, Garkavtsev I, Xu L, Hicklin DJ, Fukumura D, di Tomaso E, Munn LL, Jain RK. Kinetics of vascular normalization by VEGFR2 blockade governs brain tumor response to radiation: Role of oxygenation, angiopoietin-1, and matrix metalloproteinases. *Cancer Cell.* **6**:553-563 (2004).

Yuan F, Dellian M, Fukumura D, Leunig M, Berk DA, Torchilin VP, Jain RK. Vascular permeability in a human tumor xenograft: molecular size dependence and cutoff size. *Cancer Res.* **55**(17):3752-3756 (1995).

Chapter 2

Synthesis Work

In chapter one, the design principles for a second-generation nanocell were discussed. In pursuit of developing a nanocell drug delivery vehicle with enhanced efficiency and tumor targeting properties, a number of conjugate molecules were synthesized and analyzed. In what follows, the possibility of using chitosan in the nanocell envelope is assessed, folate receptor targeting is incorporated into the envelope polymers of the nanocell, a dendrimer-based prodrug is developed for loading the nanocell with a slow-acting cytotoxic drug, and multiple cytotoxic drug conjugates are synthesized as proof-of-concept-expandability.

2.1 Folate-Chitosan Conjugates

2.1.1 Introduction

Initially, the research focused on the creation of chitosan-based conjugates for use in the nanocell envelope. Chitosan is an established biocompatible material, and it exhibits many properties that make it an attractive choice for an envelope component.

- Chitosan is a cationic polysaccharide that has been used widely to encapsulate pharmaceuticals for transport in the bloodstream. Such properties are desirable if one expects to create a stable vesicle for transport in a hydrophilic environment such as the bloodstream.
- Chitosan also contains hydroxyl and primary aliphatic amine side groups. These groups can be used as conjugation sites in the incorporation of tumor-targeting ligands, as discussed in chapter one.
- Chitosan is very abundant in nature, and therefore it is inexpensive and easily obtained.

In the following experiments, folate was conjugated to chitosan with the eventual hope of synthesizing vesicles consisting of both chitosan and folate-chitosan conjugates. As is common procedure in liposome design, a polyethylene glycol-disteroyl phosphatidylethanolamine (PEG-DSPE) copolymer can be incorporated into the chitosan

envelope in order to avoid uptake of the liposome by the Kupffer cells of the liver, and thereby prolong nanosome circulation time and avoid [Wu and Zern, 1996].

2.1.2 Materials and Methods

Folic acid-chitosan (FA-CS) conjugates were synthesized as follows: 0.1 mmol folic acid and 0.25 mmol ethyldimethylaminopropyl carbodiimide (EDC) were dissolved in 2 mL dimethyl sulfoxide (DMSO) for 1 hour. The solution was then added to 5 mL of 1% (weight/volume) medium molecular weight chitosan (150 kDa) in 0.2 M acetate buffer (pH 4.7). In parallel, the same reaction was carried out in 0.4 M acetate buffer (pH 4.7). The reaction was quenched after 24 hrs by bringing the reaction mixture to pH 9.0 via drop wise addition of 1% sodium hydroxide. DMSO, EDC, and unreacted folic acid were removed by dialysis against phosphate buffer (pH 7.4) and water, for 2 days each. The purified product was lyophilized to yield a light yellow, fluffy solid. [Mansouri et al., 2006]

2.1.3 Results and Conclusions

The dried product was analyzed using UV absorbance spectroscopy at 368 nm. For analysis, the sample was re-dissolved in acetate buffer. To re-dissolve the samples, it was necessary to ultrasonicate them at a power of 220 watts, for approximately 15 seconds each. A comparison of the UV absorbance readings to a folic acid standard curve allowed the amount of FA-CS conjugation to be determined. Assuming that the

Sample	Initial Solvent (pH4.7)	Redissolved in (pH 5.5)	Abs. at 363 nm	Calc. [FA], mM All	Linear
MMW with EDC	0.2M acetate buffer	5 mM acetate buffer	2.8633	**0.49**	**0.39**
MMW with EDC	0.4M acetate buffer	5 mM acetate buffer	2.7942	**0.47**	**0.38**

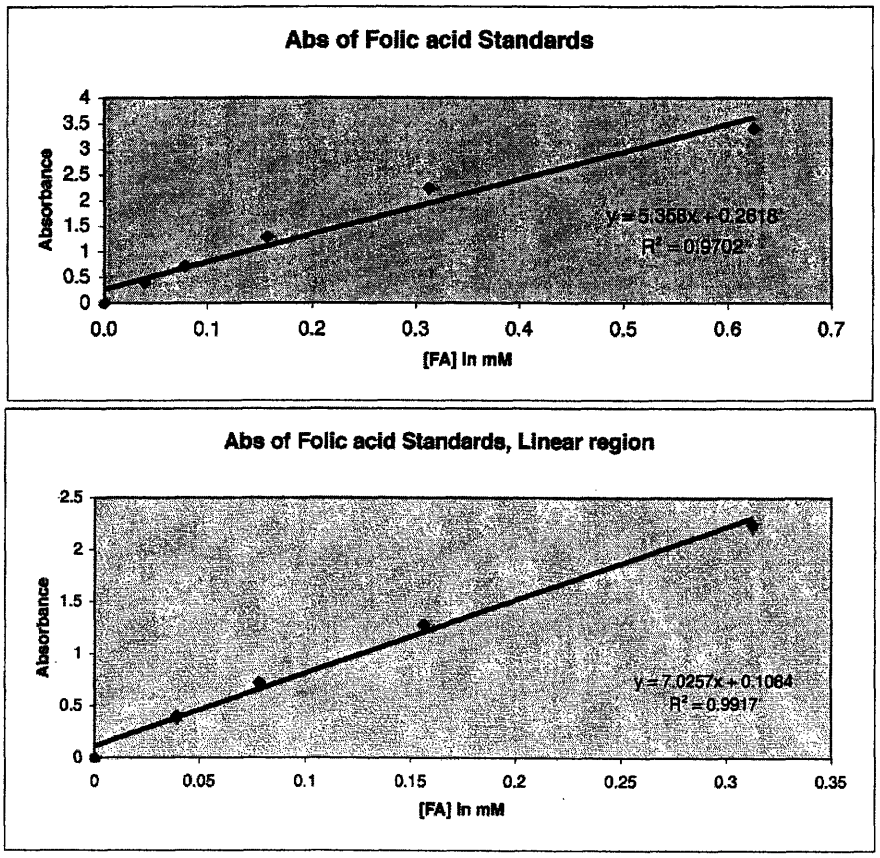

Figure 2.1: Ultraviolate absorbance (368 nm) studies of the product of the reaction to synthesiize medium molecular weight chitosan (MMW, 150 kDa) conjugated to folic acid. The reaction proceeded as described in the text, in 0.2 M and 0.4 M acetate buffers. Using the linear region of the folic acid standard curve, folic acid concentrations of 0.39 mM and 0.38 mM are observed for the reactions in 0.2 M and 0.4 M acetate buffer, respectively. 0.5 mg/ml of sample (3.33 μM) was used for the studies, implying that the conjugation efficiency was approximately one folate molecule per 7.25 chitosan (MMW) subunits. Note that the linear region does not extend beyond 0.31 mM. The system was blanked with 5 mM acetate buffer (pH 5.5), and all samples were dissolved in the same buffer.

final product was purified to contain only chitosan and FA-CS, the UV studies revealed that the conjugation succeeded, with roughly one folate molecule per 7.25 chitosan subunits (Figure 2.1).

2.2 Chitosan and Folate-Chitosan Nanosomes

2.2.1 Introduction

The goal of the research with chitosan was to use the polysaccharide to encapsulate therapeutic compounds. In accordance with this goal, the synthesis of chitosan nanosomes was attempted. The gelation method was selected for this synthesis, primarily because of its simplicity and effectiveness with chitosan.

2.2.2 Materials and Methods

The synthesis of chitosan nanoparticles was attempted following the ionic gelation method, described in [Calvo et al., 1997]. 7.1 and 7.3 mg of chitosan and FA-CS, respectively, were each added to 5 mL of 1.75 mg/mL acetic acid. The resulting mixture was ultrasonicated at 220 watts for 10-15 seconds to form a solution. To these solutions, 2 mL of 0.735 mg/mL sodium tripolyphosphate (TPP) was added drop wise. Thus, the final concentrations of chitosan, acetic acid, and TPP were 1 mg/mL, 1.75 mg/mL, and 0.21 mg/mL, respectively. The solutions were set on medium stir for 2 hrs.

2.2.3 Results and Conclusions

After the experiment completed, the solutions were analyzed by light scattering spectroscopy. Particles of a 158.4 nanometer radius were obtained for the chitosan-only protocol, and a mixture of particles with 246.2 and 1871.1 nanometer radii were obtained for the folate-chitosan protocol. Scanning Tunneling Microscopy (STM) was also attempted, though it revealed chitosan clumps rather than nanoparticles. However, it should be noted that a lyophilizer was used to transition the nanoparticle to the solid phase for the STM experiments; it is likely that the process of lyophilization caused the destruction of the nanoparticles.

Though light scattering spectroscopy did return a reasonable radius for the particles in solution, it cannot be used to infer that the particles are indeed spherical and/or hollow. For this matter, a direct form of visualization, such as transmission electron microscopy (TEM), is required. However, assuming that the nanoparticles were of the desired shape, they were still larger than desired. The final size of the nanoparticles is highly dependent on the concentrations of chitosan and TPP in the gelation method [Calvo et al., 1997], so further experiments would be necessary in order to optimize the gelation method to our needs.

In general, working with chitosan was difficult. As mentioned previously, it was often necessary to use ultrasonication when dissolving the chitosan conjugates. Unfortunately, the energy introduced by ultrasonication readily breaks polysaccharide chains, and therefore introduces additional variables to the experiment [Tang et al., 2003]. In addition to being a studied side effect of ultrasonication, the breakage of the

polysaccharide manifested experimentally, in the inconsistently sized chitosan nanoparticles.

The size inconsistency discussed would introduced uncertainty in nanocell loading and therefore in the dosage of the delivered drugs. Thus, the immediate benefit of using chitosan did not outweigh the difficulty of working with the material, and a decision was made to forego the use of chitosan and to focus on incorporating folate receptor targeting into the original nanocell envelope.

2.3 Cisplatin Analogue and PLGA Conjugate

2.3.1 Introduction

Cisplatin is an established cytotoxic drug that is used in the treatment of some types of cancer. The biomolecule induces apoptosis in cells by binding to a number of targets, including DNA, cell membrane phospholipids, and different cytoplasmic and membrane proteins [Gonzales et al., 2001; Fuertes et al., 2003]. In this study, an analog was synthesized and bound to PLGA. The conjugate serves as another novel cytotoxic conjugate that may be used in constructions of engineered particles such as the nanocell. The research on the cisplatin-analog conjugate was lead by and is continuing in the hands of Dr. Geeti Gangal.

2.3.2 Materials and Methods

Step 1: 1,3-dibromo-2-propanol was stirred with sodium azide in a 1:3 molar ratio, in anhydrous dimethylformamide (DMF) as the solvent (15 mL DMF per 1g 1,3-dibromo-2-propanol). The reaction was carried out at 50°C for 24 hrs, after which the product was extracted using ethyl acetate and washed 3x each with water and brine (10%). The solvent was evaporated to yield 1,3-diazido-2-propanol (see Figure 2.2).

Step 2: 1g of 1,3-diazido-2-propanol was reacted with 150g 10% Pd/C catalyst in 100 mL methanol under hydrogen atmosphere. The reaction was monitored using TLC (3:1 hexane:ethyl acetate, then dipped in ninhydrin and heated) and carried out until completion (7-8 hrs). Purification yielded 1,3-diamino-2-propanol (see Figure 2.2).

Step 3: 1,3-diamino-2-propanol was dissolved in water (50 mg/mL) and treated with potassium tetrachloroplatinate in 1:1 molar ratio. The solution was filtered and then stirred for 24 hrs at room temperature. Refrigeration for 24 hrs resulted in the precipitation of a yellow-brown solid – the cisplatin analogue – which was filtered and dried.

Step 4: A cisplatin-PLGA conjugate was synthesized in the following way. 37.8 mmol (1 equiv.) of activated poly(lactic-co-glycolic acid) was dissolved in DMF (30 mg/mL) under nitrogen atmosphere. To the solution, 1.6 equiv cisplatin analogue, 1 equiv. 4-dimethylaminopyridine (DMAP) and 4 equiv. of triethylamine (TEA) were added. The reaction was carried out under nitrogen atmosphere for 24 hrs. The reaction solution was added drop wise to 100 mL diethyl ether in order to precipitate the product.

After allowing the ether to stir slowly overnight, in the dark, the ether was decanted and the product was re-dissolved in methylene chloride. The resulting solution was washed twice in a 0.1% HCl + 10% brine solution, dried, and re-precipitated in ether. After slow stirring overnight, the ether was decanted. The product was collected in vials and placed in a vacuum desiccator to dry.

2.3.3 Results and Conclusions

A cisplatin analogue and its PLGA conjugate were successfully synthesized, and testing to determine the biological activity of both will be performed outside of the scope and timeframe of this thesis. The conjugate represents a move to incorporate different cytotoxic drugs into the nanocell framework. Such testing is necessary because cancer is a highly variable disease – unique treatments are necessary for different types of tumors. In the context of the nanocell, it is important to keep in mind that this variability affects all layers of the nanocell: differing tumor types express different cell surface receptors, respond to different anti-angiogenesis drugs, and have varying sensitivities to the plethora of cytotoxic compounds available [Yong et al., 2006; Undevia et al., 2005]. The medical literature is an excellent guide to such variation, and the matching treatments currently used.

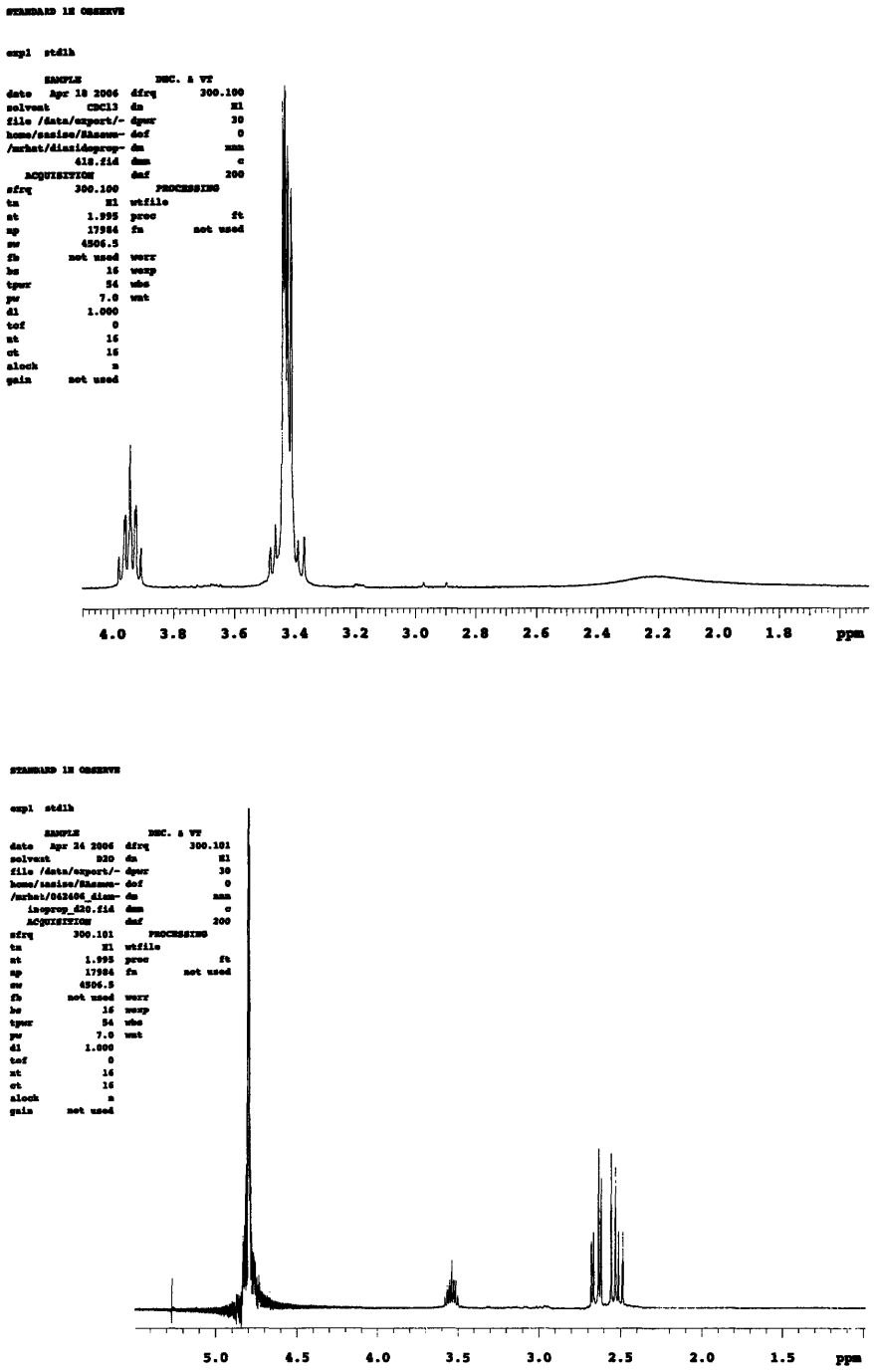

Figure 2.2: Proton NMR confirmation of successful steps towards the synthesis of a cis-platin analogue. The synthesis of 1,3-diamino-2-propanol from 1,3-diazido-2-propanol was confirmed by the appearance of the coupled double doublets at $\delta = 2.59$ ppm and the conversion of a quintet at $\delta = 3.95$ ppm to a septet at $\delta = 3.54$ ppm.

2.4 FA-PEG-DSPE Conjugates

2.4.1 Introduction

In designing the envelope of the nanocell, several factors must be taken into account. First, the envelope must be hydrophobic enough in order stably encapsulate therapeutics in a manner reminiscent of a cell membrane. Second, the nanocell should remain stable in the blood stream. Second, the lipophilicity of the nanocell must be controlled such that it is not rapidly endocytosed by the Kupffer cells of the liver.

In the pilot project, polyethylene glycol (PEG) – disteroyl phosphatidyl-ethanolamine (DSPE) copolymers were incorporated into the envelope in order to decrease the nanocell's surface hydrophobicity. When used in liposomes, the copolymer introduces a negative surface charge [Webb et al., 1998]. Thus, our goal in this portion of the research was to develop a tumor targeting FA-PEG-DSPE conjugate that could be used in the envelope of the next-generation nanocell.

2.4.2 Materials and Methods

Synthesis of FA-PEG-NH_2 (Figure 2.3): FA-PEG-NH_2 was synthesized from bis(aminoethyl) PEG in the following way. 0.1 mmol (200 mg) of bis(aminoethyl) PEG was dissolved in 2 mL DMSO with 4 μL pyridine. 1 molar equivalent of folic acid and dicyclohexylcarbodiimide (DCC) were added to the reaction vial, and the solution was

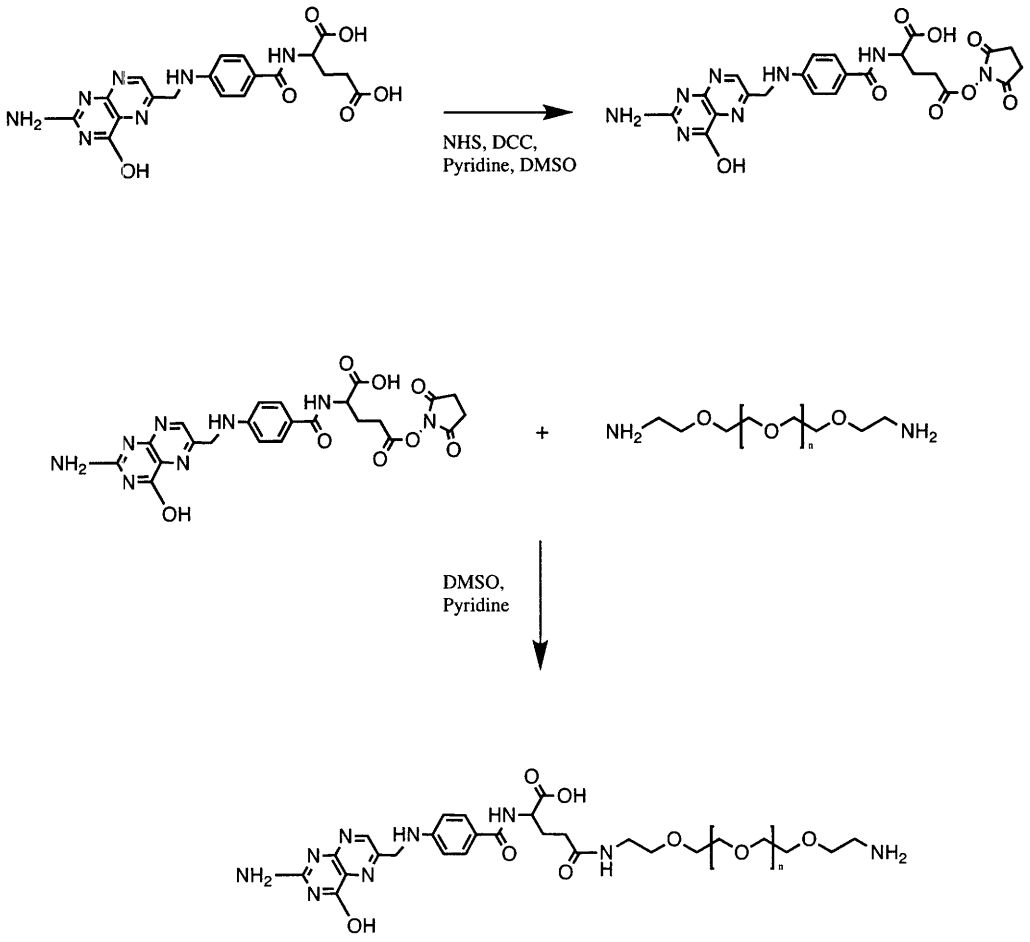

Figure 2.3: Proposed reaction route for the synthesis of the FA-PEG-NH_2 conjugate.

stirred in the dark for 24 hrs. After 24 hrs, 2 mL water was added to the reaction, dicyclohexylurea (DCU) was precipitated from solution. DCU was removed by filtration, and the filtrate was then dialyzed against 5 mM ammonium bicarbonate (pH 9.0) and water. After dialysis, the product was lyophilized to remove excess solvent. [van Steenis JH et al., 2003]

To purify FA-PEG-NH_2 from bis(aminoethyl) PEG, a cellulose phosphate cation exchange resin was prepared. Initially, column chromatography purification was attempted using the column. The product formed a visible yellow band, but it did not elute with varying concentrations (up to 10 mM) of ammonium bicarbonate as the eluant. Later, a batch adsorption technique was used: the lyophilized product was mixed with the prepared cellulose phosphate resin in 10 mM ammonium bicarbonate for 1 hr. The mixture was then centrifuged and filtered to remove the cellulose phosphate, and lyophilized to yield a light yellow solid (9.6 mg).

Synthesis of FA-PEG-NHS (Figure 2.4): Following the synthesis of FA-PEG-NH_2, the synthesis of FA-PEG-NHS was attempted. FA-PEG-NH_2 was dissolved in DMSO at a concentration of 10 mg FA-PEG-NH_2 per (1 mL DMSO + 0.8 μL TEA). To this solution, 10 equiv. of disuccinimidyl suberate (DSS) was added, and the reaction was carried out overnight, in the dark. To isolate the product, the reaction mixture was added drop wise to ether and stirred slowly for 3.5 hrs. The ether was decanted, and the remaining precipitate was re-dissolved in methylene chloride. After vacuum evaporation to remove methylene chloride, a clear, oily liquid remained. However, this liquid was not the desired product (see results section).

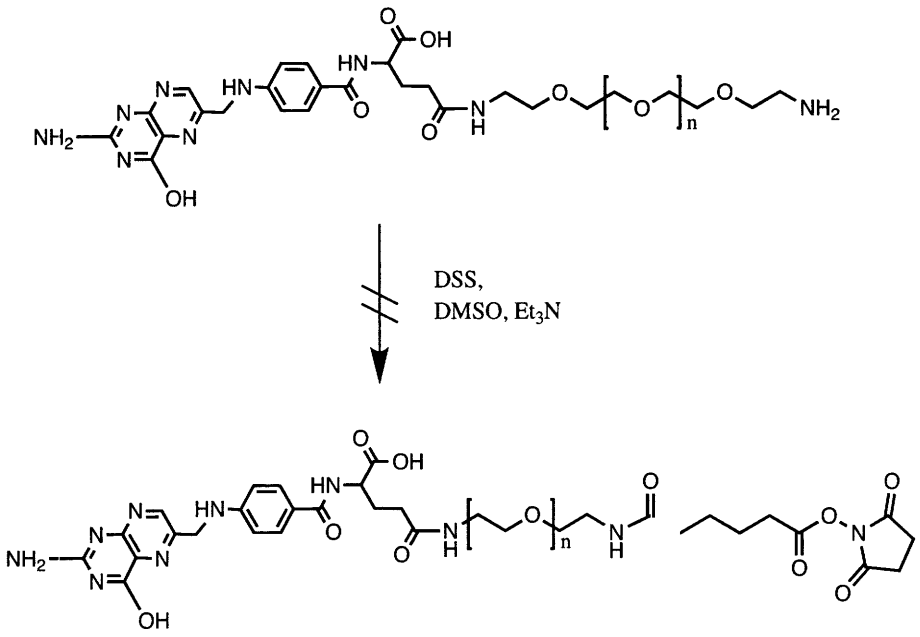

Figure 2.4: Proposed reaction route for the synthesis of the FA-PEG-NHS conjugate. The reaction did not occur.

Synthesis of N-succinyl DSPE: The synthesis of N-succinyl DSPE was attempted by mixing 100 mg DSPE (1 equiv.) and 1.1 equiv. of succinic anhydride in 5 mL chloroform, with 1μL pyridine per 1 mL chloroform. However, DSPE and succinic anhydride did not dissolve in chloroform or in a variety of chloroform:methanol solutions. The reactants were allowed to react overnight, as a mixture, but no reaction was observed. No reasonable amount of pure product could be obtained from the solution component of the mixture. Instead, the starting material was recovered and stored. It was hoped that the synthesis depicted in Figure 2.5 could be executed. [Lee and Low, 1995].

Synthesis of FA-PEG-DSPE: Ultimately, FA-PEG-DSPE was synthesized from purchased NH_2-PEG-DSPE [Gabizon et al., 1999]. 7.1 μmol NH_2-PEG-DSPE and 1.75 equiv. of folic acid were dissolved in 200 μL and 100 μL DMSO, respectively. 100 μL pyridine and the folic acid solution were added to the reaction flask containing NH2-PEG-DSPE. Shortly afterwards, 4.5 equiv. of DCC was added, and the reaction was stirred in the dark and monitored using TLC. The reaction was completed after 5.5 hrs. Water was added to the reaction flask, and DCU was precipitated from solution. DCU was removed by centrifugation (9000 RPM, 5 min), and the remaining unwanted reaction material was removed by dialysis against 50 mM sodium chloride and water. The full reaction route is shown in Figure 2.5.

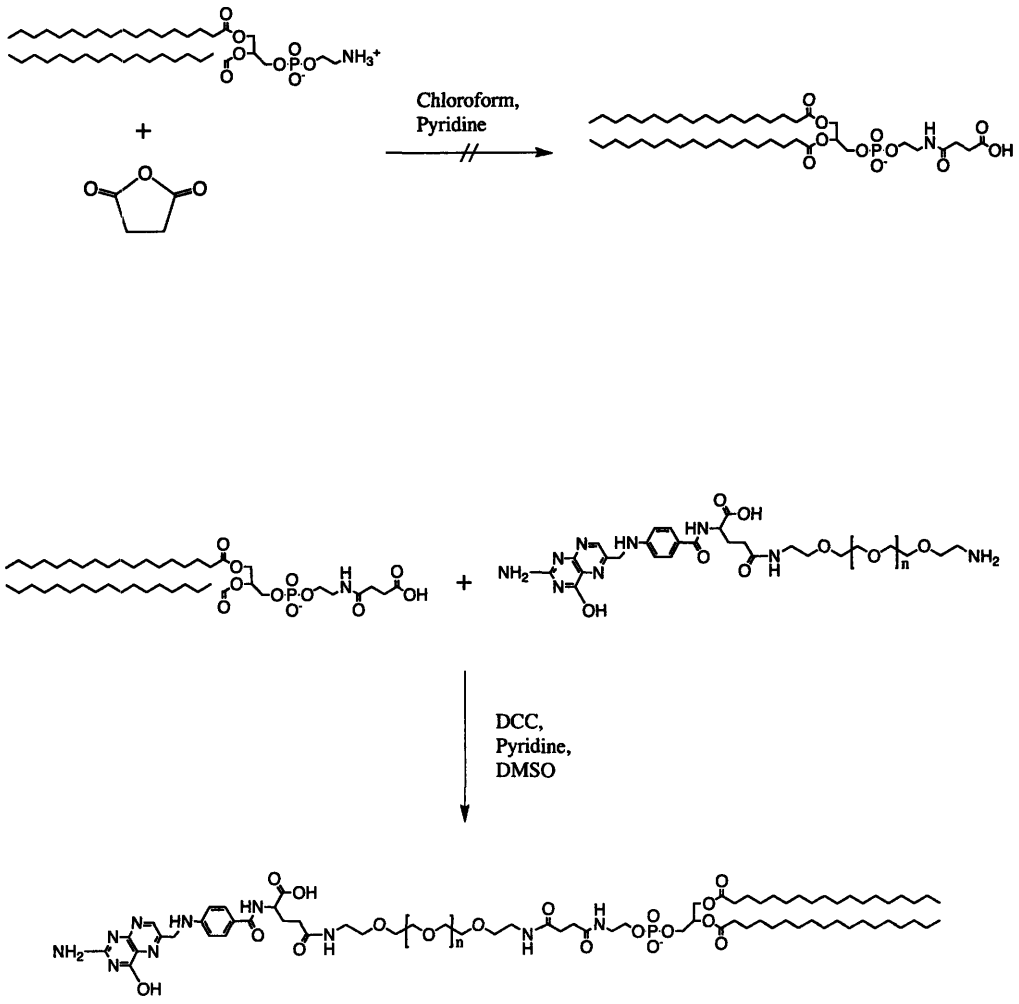

Figure 2.5: Proposed reaction route for the synthesis of the FA-PEG-DSPE conjugate. The upper reaction did not occur.

	Abs of sample
	2.2525
[FA] calc:	0.29 mM

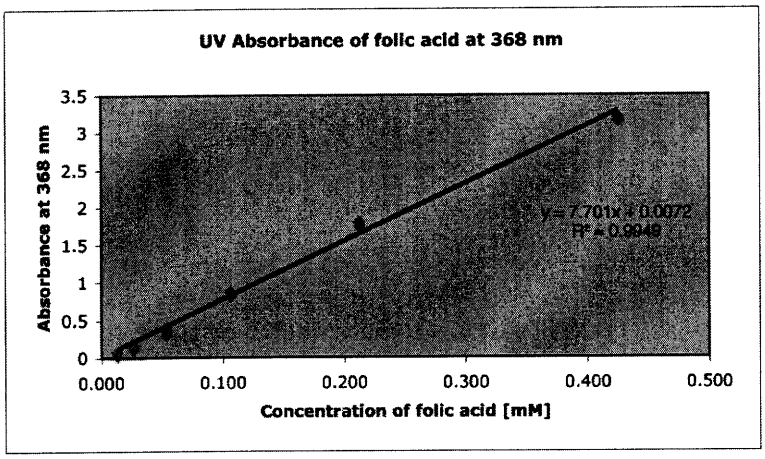

Figure 2.6: Ultraviolate absorbance (368 nm) studies of the product of the reaction to synthesiize FA-PEG-NH_2. The concentration of folic acid was determined to be 0.29 mM. The system was blanked with 10 mM ammonium bicarbonate buffer (pH 8.85), and all samples were dissolved in the same buffer.

FA-PEG-NH_2 (0.7 mg/ml)	2.1488
FA-PEG-DSPE (0.7 mg/ml)	0.9309

Calc. [FA], FA.PEG.NH_2	Calc. [FA], FA.PEG.DSPE
0.34 mM	0.14 mM
[FA], 100% FA.PEG.NH_2	[FA], 100% FA.PEG.DSPE
0.29 mM	0.22 mM

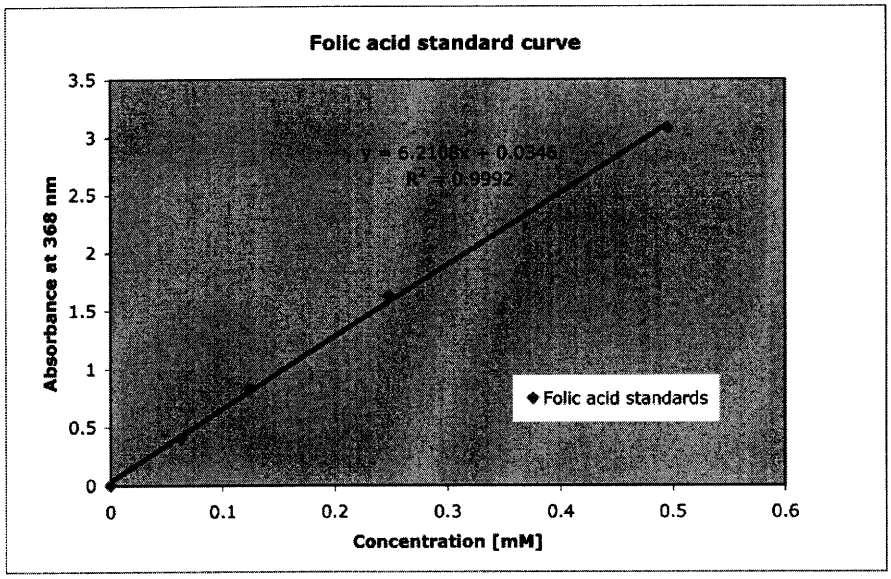

Figure 2.7: Ultraviolate absorbance (368 nm) studies of the product of the reactions to synthesiize FA-PEG-NH_2 and FA-PEG-DSPE. The concentrations of folic acid were determined to be 0.34 mM and 0.14 mM, respectively. Sample concentrations of 0.7 mg/ml were used in the studies – one would expect the observed concentrations of folic acid in the FA-PEG-NH_2 and FA-PEG-DSPE samples to be 0.29 mM and 0.22 mM, respectively, in the case of a 1:1 folic acid:polymer conjugation. Thus, conjugation efficiencies of approximately 117% and 63% (FA-PEG-NH_2 and FA-PEG-DSPE, respectively) were obtained; implicit is the over-conjugation of NH_2-PEG-NH_2 (monoconjugation was desired). The system was blanked with 10 mM ammonium bicarbonate buffer (pH 8.85), and all samples were dissolved in the same buffer.

2.4.3 Results and Conclusions

The purified, folate-conjugated solid was analyzed using UV absorbance spectroscopy (368 nanometer wavelength) in conjunction with a linear folic acid standard curve. The analysis suggested that 71-72% of the final solid in the FA-PEG-NH_2 synthesis was successfully folate conjugated (see Figure 2.6); the remaining 30% of the sample was either bis(aminoethyl) PEG, light-exposed FA-PEG-NH_2, or other impurity. Additionally, some of the folate-conjugated solid may have been doubly conjugated. Indeed, a repeat synthesis, in which the reaction proceeded for six additional hours and under well-maintained darkness, resulted in a conjugation efficiency of 117% (Figure 2.7).

A UV absorbance scan was performed on the product of the FA-PEG-NHS synthesis in order to determine if either one of folate or the NHS active group was present. The scan revealed that none of the expected absorbance peaks were present. If the product were FA-PEG-NHS, absorbance peaks would have been observed at 270 and 368 nanometer wavelengths, due to the NHS and folate groups, respectively.

UV absorbance spectroscopy at 368 nanometers was also used to analyze the product of the FA-PEG-DSPE synthesis. Under the assumption that the final product was purified well enough to be only FA-PEG-DSPE or NH_2-PEG-DSPE, the UV studies suggested that 63% of the product was folate-conjugated (see Figure 2.7).

The yield of the reaction FA-PEG-NH_2 synthesis reaction was very low, and the subsequent FA-PEG-NHS step did not proceed as expected. After the purification of FA-PEG-NH_2 and the synthesis of N-succinyl DSPE from basic components proved to be

difficult, a decision was made to synthesize the envelope components using starting materials that are closer to the desired product (i.e. NH_2-PEG-DSPE, as described above).

2.5 Methotrexate-PAMAM Prodrug

2.5.1 Introduction

In the drive to develop an effective and efficient way to load the nanocell with slow-release cytotoxic drugs, dendrimers offer many unique capabilities. First, because dendrimers are highly branched molecules with numerous terminal groups, they can bind several ligands per molecule. For example, a single third generation PAMAM dendrimer can bind a theoretical maximum of thirty-two terminal ligands, whereas a linear molecule can bind only two such ligands. Second, because dendrimers are highly symmetric and are synthesized in a controlled manner, there is minimal variation in the final size of the dendrimer-drug conjugate. In the following experiments, methotrexate (MTX) was conjugated to a third generation PAMAM dendrimer to form a prodrug. An ester bond anchors MTX to the dendrimer; esterase enzymes in tissue readily cleave this bond. Because esterase enzymes are upregulated when cells are stimulated to degrade the extracellular matrix and migrate, as they do in hypoxic tumor microenvironments [Pennacchietti S. et al., 2003], the dendrimer should display the preferential release of methotrexate in the hypoxic environment brought about by anti-angiogenesis therapy.

2.5.2 Materials and Methods

2.84 μmol of a third generation PAMAM dendrimer with terminal hydroxyl groups was dissolved in 165 μL anhydrous DMF. Separately, 32 equiv. methotrexate (MTX) and 32 equiv. CMPI were dissolved in 500 μL and 165 μL of anhydrous DMF, respectively. The MTX solution was added to the dendrimer solution, and 64 equiv. triethylamine (TEA) was added to the reaction mixture. The CMPI solution was then added, and the reaction was stirred for 24 hrs at 40°C. After 24 hrs, the reaction mixture was dialyzed against 10 mM ammonium bicarbonate buffer to purify the dendrimer conjugates. During dialysis, a brown precipitate formed periodically, and was broken up manually. After dialysis, the product was lyophilized to yield a brown solid. The reaction route is shown in Figure 2.8.

2.5.3 Results and Conclusions

The PAMAM-MTX conjugate was analyzed using UV absorbance spectroscopy at a 380-nanometer wavelength and a linear methotrexate standard curve. UV spectroscopy showed approximately 68% conjugation (see Figure 2.9), and NMR spectroscopy corroborated these results (see Figure 2.10). A repeat experiment demonstrated similar conjugation efficiencies. Transmission electron microscopy showed that the PAMAM-MTX conjugates were all approximately 10-12 nanometers in diameter (see Figure 2.11), and displayed radial symmetry, as expected.

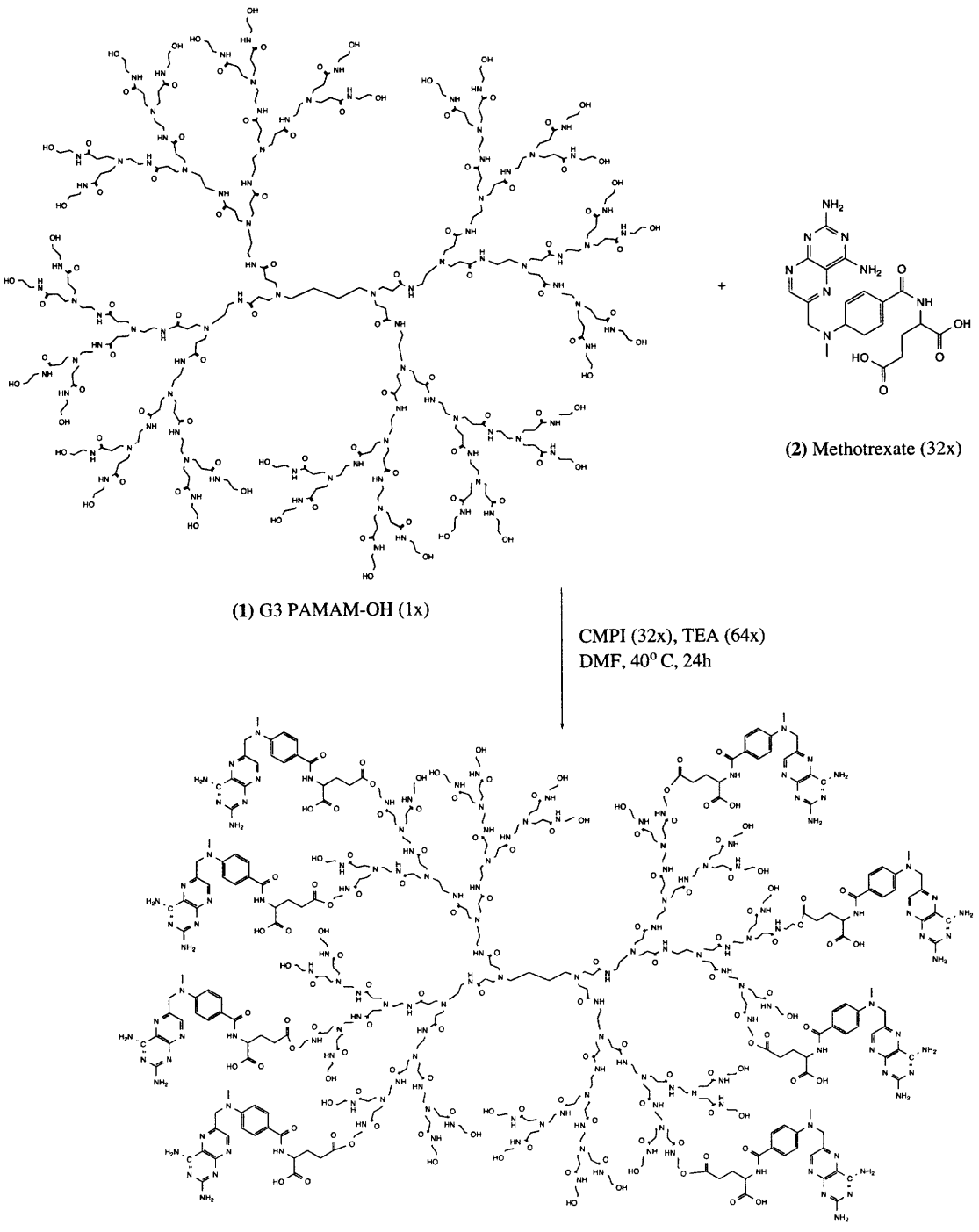

Figure 2.8: The proposed reaction route for the conjugation of methotrexate to a G3 polyamidoamine dendrimer. Note that not all of the thirty-two potential methotrexate ligands are shown in the final conjugate – have of the ligands are omitted for ease of display.

	Absorbance at:		Calculated MTX [mg/ml] from:			
Sample [mg/ml]	300 nm	380 nm	300 nm data	%	380 nm data	%
0.019	0.5778	0.1706	0.012	63%	0.013	68%
0.038	1.0681	0.3377	0.022	59%	0.026	68%
0.075	2.0239	0.6811	0.043	57%	0.052	69%
0.150	Out of	1.3688	n/a	n/a	0.105	70%
0.300	range	2.6818	n/a	n/a	0.206	69%

**300 nm data is nonlinear*

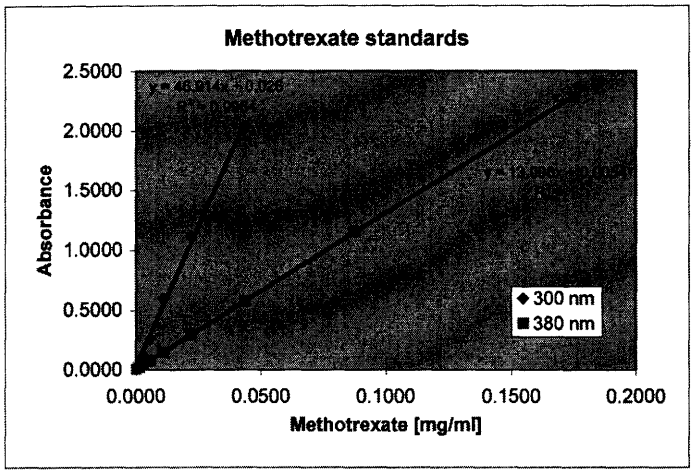

Figure 2.9: Ultraviolate absorbance studies of the product of the reactions to synthesiize the methotrexate-(G3)polyamidoamine conjugate. The absorbance studies were conducted at 300 and 380 nm. However, only the 380 nm data set provided an usable methotrexate standard curve. After testing the absorbance of several different dilutions of the sample (throughout the range of the standard curve), the conjugation efficiency of the reaction was determined to be approximately 69%. The efficiency was highly reproducible (data not shown), indicating that further conjugation was likely hindered by steric effects. The system was blanked with DMSO, and all samples were dissolved in DMSO.

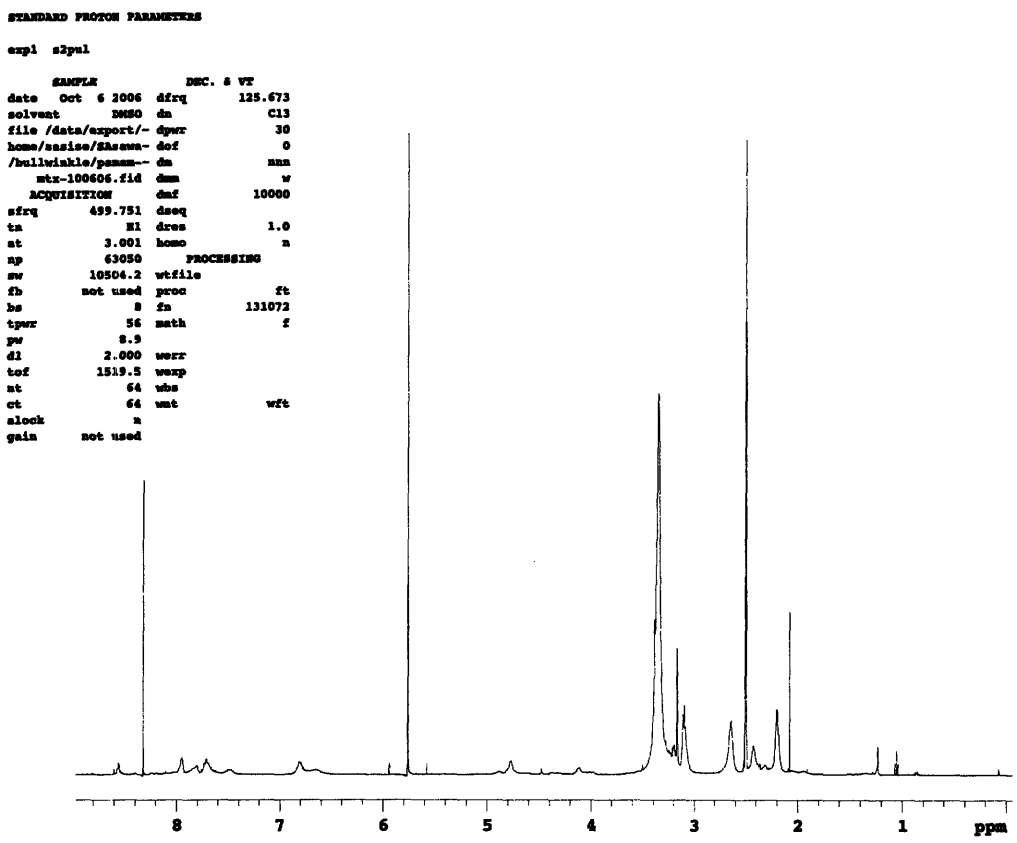

Figure 2.10: Proton NMR studies of the methotrexate–(G3)polyamidoamine conjugate. The results of the ultraviolet studies are confirmed by integration of the small peaks: the ratio of the terminal hydroxyl signal (broad ^{1}H-shift peak at δ = 4.78 ppm), representing the unconjugated terminal end of the polyamidoamine dendrimer, to an aromatic C-NH_2 signal (one of the two broad ^{1}H-shift peaks between δ = 6.65 ppm and 6.9 ppm), representing methotrexate ligand, is approximately 0.45.

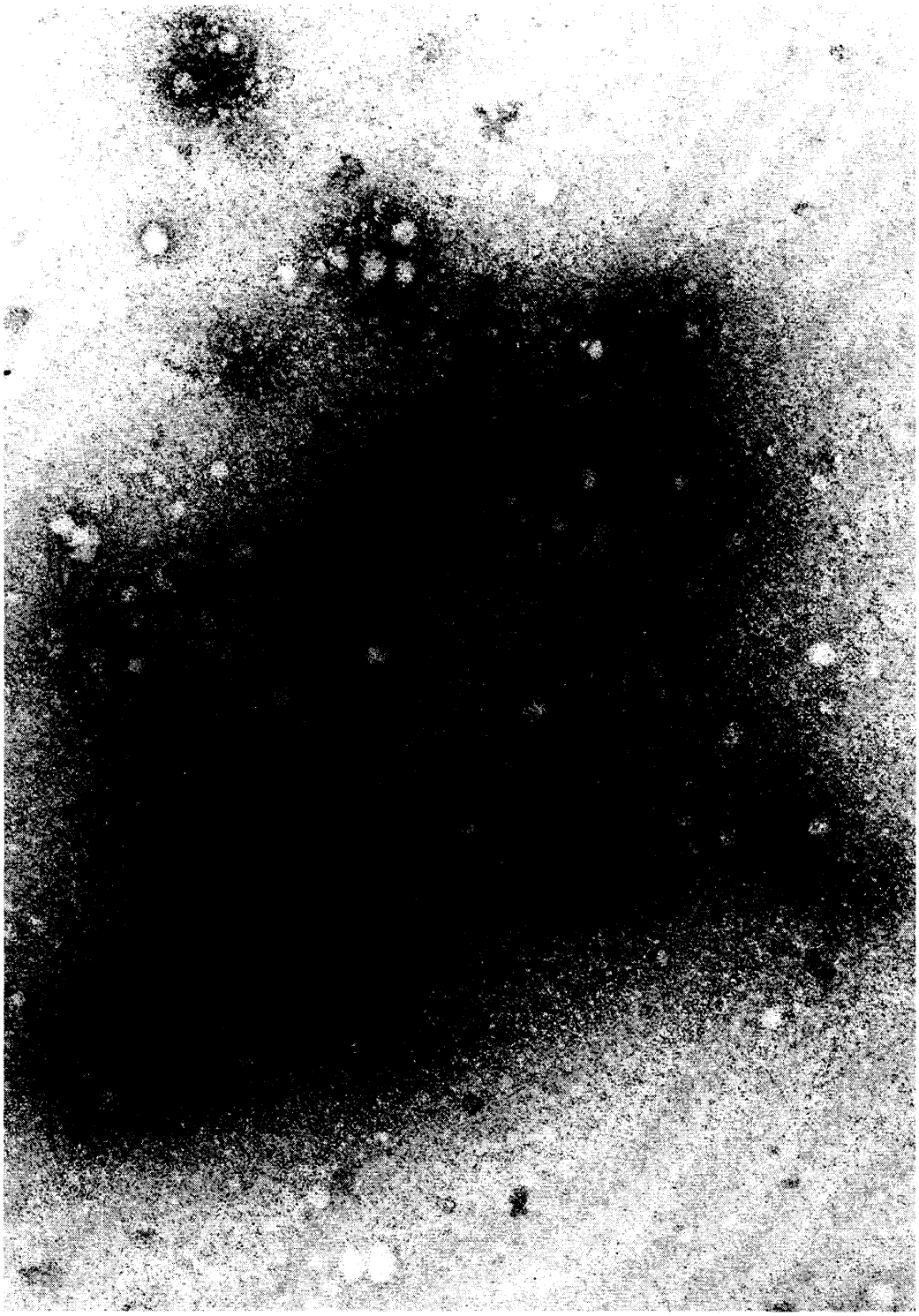

Figure 2.11: Transmission electron microscopy of the methotrexate–(G3)polyamidoamine conjugate. The x-axis scale is 300 nm. The conjugates, as shown, have radial symmetry and range from 10-12 nm in diameter.

The PAMAM-MTX conjugation was successful, though not 100% efficient. It is likely that steric effects prevented the complete conjugation of thirty-two methotrexate molecules to each PAMAM dendrimer. In cell studies performed by Dr. Sujan Kabir, which will be described in chapter three, the conjugate was shown to have anti-tumor cell activity. Additionally, the dendrimer prodrug showed enhanced potency in hypoxic cellular environments. Thus, in addition to developing an efficient cytotoxic drug-carrier for the loading of the nanocell, another layer of spatial targeting was successfully incorporated into the nanocell design. Though each spatial tumor targeting layer in the nanocell – selective extravasation, receptor targeting, and hypoxia-enhanced drug release – is by no means 100% specific to the tumor microenvironment, each tumor-preferring layer should build upon the others to improve the therapeutic index of the nanocell.

2.6 PD98059 Amide Linkage to Aromatic Amine

2.6.1 Introduction

To further develop cytotoxic dendrimer-based prodrugs similar to the MTX conjugate described above, the conjugation of a MAPK kinase inhibitor, PD98059, to PAMAM was explored. In evaluating possible reaction routes, the basic requirement was that the reaction result in the formation of an ester bond. As discussed above, an ester bond would allow for the *in vivo* esterase-mediated release of the bound drug.

Several reactions were considered and/or tested, and rejected on the basis of difficulty and potential toxicity. Ultimately, it was decided that a conjugation reaction involving the sulfhydryl-activation of the amine group of PD98059 would be ideal. After the activation step, the prodrug can be synthesized via a conjugation reaction involving a heterobifunctional (maleimide-*N*-hydroxysuccinimide) crosslinker, activated PD98059, and the PAMAM dendrimer.

2.6.2 Materials and Methods

The PD98059 activation was carried out as follows. 0.0374 mmol PD98059 was dissolved in 400 μL DMSO. To the resulting solution, 1 equiv. TEA and 10 equiv. 2-iminiothiolane-HCl was added, and the reaction was stirred and monitored by TLC. After 24 hrs, the reaction mixture was dialyzed against 25 mM sodium borate buffer (pH 9.0) and water for 2 days each. The resulting mixture was lyophilized and analyzed with NMR spectroscopy.

2.6.3 Results and Conclusions

TLC monitoring showed that the activation of PD98059 occurred slowly. However, the reaction did occur, as can be confirmed by the appearance of a sulfhydryl peak in the ^{1}H NMR spectrum of the product (see Figure 2.12). In conjugating different drugs to the dendrimer, careful consideration must be given to both the cross-linker used and the reaction route taken to conjugation. The cross-linker and reaction route must

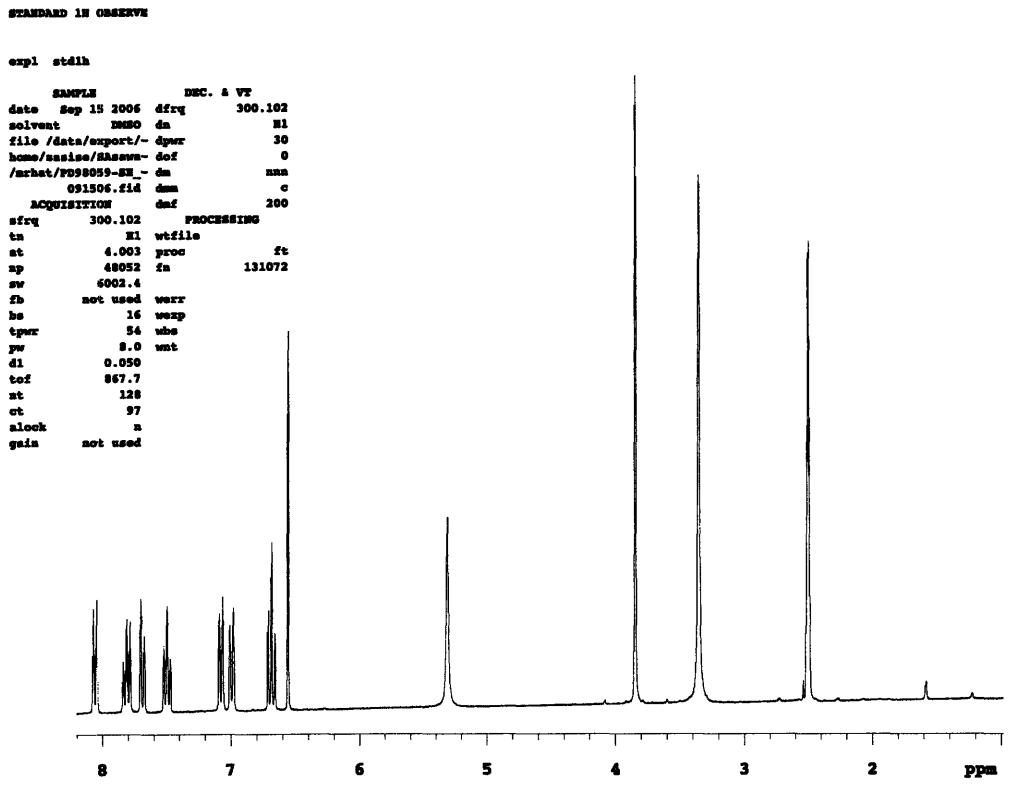

Figure 2.12: Proton NMR study of the cytotoxic compound PD98059, a MAPK kinase inhibitor, after being activated with a sulfhydryl group. The reaction did not go to completion, but the appearance of a ^{1}H peak at 1.59 ppm on the NMR spectrum above indicates the successful sulfhydryl activation of PD98059. Upon successful activation, PD98059 may be conjugated to the G3 polyamidoamine dendrimer via an ester bond by using any one of a number of heterobifunctional crosslinkers (i.e. maleimidoethyl succinimidyl succinate).

allow for a reaction of acceptable efficiency to take place, an ester bond to be formed somewhere between the drug and the dendrimer, and for the cytotoxic compound to maintain its bioactivity upon its esterase-mediated cleavage from the dendrimer.

2.7. Summary

The work described above has focused on the synthesis of the basic components of the second-generation nanocell. The initial objective to use chitosan in the nanocell envelope was abandoned due to the difficult and time-consuming task of working with the material. Furthermore, the non-economic benefits of using chitosan were not entirely unique: a biocompatible envelope had already been designed and synthesized in the pilot study. As such, the focus of the research shifted from developing a chitosan-based envelope to incorporating folate receptor targeting into the original nanocell envelope. To incorporate folate receptor targeting into the original envelope, different synthetic routes to the desired conjugates were considered. Ultimately, the synthesis of FA-PEG and FA-PEG-DSPE conjugates succeeded, and was found to be most efficient and economical with fewer reaction steps. Upon synthesizing these conjugates, the research shifted to developing a novel loading mechanism for the nanocell.

To achieve the goal of creating a more efficient loading mechanism, a dendrimer-based prodrug was synthesized. Methotrexate was conjugated to a third-generation PAMAM dendrimer through an ester bond with a reproducible efficiency of 70%; the dendrimer-drug conjugates were 10-12 nanometers in diameter and bioactive. Reaction

routes to linking other cytotoxic drugs (i.e. PD98059) to the dendrimer via an ester bond were also explored and identified. The dendrimer prodrug, combined with the folate receptor-targeting envelope, stands to advance the nanocell to a unique level of effectiveness. In the following chapter, the denrimer prodrug is shown to be bioactive, while also displaying preferential release of the bound cytotoxic drug in hypoxic microenvironments.

The robustness in the design of the nanocell is extremely important. As mentioned earlier, different tumors and different individuals require uniquely optimized treatments. Such is the nature of today's increasingly personalized form of medical treatment, and the nanocell must accommodate. Accordingly, any receptor-targeting ligand that can be linked to hydroxyl or amine functional groups, either on its own or using a crosslinker, can be incorporated into the envelope of the nanocell. Similarly, any cytotoxic drug that can be conjugated via an ester bond to the hydroxyl functional group of the dendrimer can be used in the present design of the nanocell. Thus, incorporating a variety of treatments into the framework of the nanocell is a matter of chemistry, while the underlying strategic design of the nanocell may remain constant.

Bibliography

Calvo P, Remuñán-López C, Vila-Jato JL, Alonso MJ. Novel hydrophilic chitosan-polyethylene oxide nanoparticles as protein carriers. *J Appl Poly Sci.* **63**:125-132 (1997).

Fuertes MA, Castilla J, Alonso C, Perez JM. Cisplatin biochemical mechanism of action: from cytotoxicity to induction of cell death through interconnections between apoptotic and necrotic pathways. *Curr Med Chem.* **10**:257-266 (2003).

Gabison A, Horowitz AT, Goren D, Tzemach D, Mandelbaum-Shavit F, Qazen MM, Zalipsky S. Targeting folate receptor with folate linked to extremities of poly(ethylene glycol)-grafted liposomes: in vitro studies. *Bioconj Chem.* **10**(2):289-298 (1999).

Gonzalez VM, Fuertes MA, Alonso C, Perez JM. Is cisplatin-induced cell death always produced by apoptosis? *Mol Pharmacol.* **59**:657-663 (2001).

Lee RJ and Low PS. Folate-mediated tumor cell targeting of liposome-entrapped doxorubicin in vitro. *Biochim et Biophys Acta.* **1233**:134-144 (1995).

Mansouri S, Cuie Y, Winnik F, Shi Q, Lavigne P, Benderdour M, Beaumont E, Fernandes JC. Characterization of folate-chitosan-DNA nanoparticles for gene therapy. *Biomaterials.* **27**:2060-2065 (2006).

Pennacchietti S, Michieli P, Galluzzo M, Mazzone M, Giordano S, Comoglio PM. Hypoxia promotes invasive growth by transcriptional activation of the *met* protooncogene. *Cancer Cell.* **3**:347-361 (2003).

Tang ES, Huan M, Lim LY. Ultrsonication of chitosan and chitosan nanoparticles. *Int J Pharm.* **256**(1-2):103-114 (2003).

Undevia SD, Gomez_Abuin G, Ratain MJ. Pharmacokinetic variability of anticancer agents. *Nat Rev Cancer.* **5**(6):447-458 (2005).

van Steenis JH, van Maarseveen EM, Verbaan FJ, Verrijk R, Crommelin DJA, Storm G, Hennink WE. Preparation and characterization of folate-targeted pEG-coated pDMAEMA-based polyplexes. *J Con Rel.* **87**:167-176 (2003).

Webb MS, Saxon D, Wong FMP, Lim HJ, Wang Z, Bally MB, Choi LSL, Cullis PR, Mayer LD. Comparison of different hydrophobic anchors conjugated to poly(ethylene glycol): effects on the pharmokinetics of liposomal vincristine. *Biochim et Biophys Acta.* **1372**:272-282 (1998).

Wu J and Zern MA. Modification of liposomes for liver targeting. *J Hepatology.* **24**:757-763 (1996).

Yong WP, Innocenti F, Ratain MJ. The role of pharmacogenetics in cancer therapeutics. *Br J Clin Pharmacol.* **62**(1):35-46 (2006).

Chapter 3

Cell Studies

Following the synthesis of the methotrexate-(G3)polyamidoamine dendrimer described in chapter two, cell studies were performed to assess the biological activity of the prodrug. The studies were designed and executed by Dr. Sujan R. Kabir. The studies reveal that the prodrug does indeed have a cytotoxic effect, and this effect is enhanced in hypoxic cellular microenvironments. The studies were performed on Lewis Lung Carcinoma cells.

3.1. Protocol

The protocol developed by Dr. Kabir was performed on Lewis Lung Carcinoma cells purchased from ATCC (#CRL-1642). The medium used was 90% Dulbecco's modified Eagle's medium (with 4 mM L-glutamine and 1.5 g/L sodium bicarbonate) and 10% fetal bovine serum. The stock solution is typically prepared using 450 mL DMEM high glucose, 50 mL fetal bovine serum, 5 mL sodium bicarbonate, 5 mL glutamine, and

5 mL pen-strep. Upon mixing, the stock solution is filtered through a 0.45 micron filtration unit and stored at 40 °C.

The flasks used for growing and maintaining the cells is pretreated for 4 hours with a sterile 0.1% cell culture gelatin solution in deionized water; the gelatin is aspirated before plating the cells. A 85-90% confluent cell source flask is trypsized with 1 mL solution, and after 1-2 minutes, the trypsin is neutralized with 6-7 mL of LLC media. The mixture is made homogenous by pipetting. The cell solution is spun down at 2000 rpm for 5 minutes, and the pellet is resuspended in 6-7 mL media. Cells are counted, and 2.5 x 205 cells are plated in a new gelatin-coated flask. After the cells become confluent (typically 2-3 days), plating for the experiment may begin.

In plating Lewis Lung Carcinoma (LLC) cells, two flasks are used: one with normal LLC cells in media, and second with hypoxic LLC cells. Hypoxia is induced via the incubation of normal LLC cells in media with 100 μM $CoCl_2$ for 12-16 hours before plating.

For the experiment, different 96 well plates are used. The plates are pretreated for 4 hours with sterile solution of 0.1% cell culture gelatin in deionized water; the gelatin solution is aspirated before plating. In each well, 1000 LLC cells are plated in 100 μM media, and the cells are incubated for 6 hours in order to allow attachment. At time point zero, the cells are treated with DMSO, free and conjugated methotrexate (DMSO is the vehicle).

The cells are treated with control (zero), 0.001, 0.01, 0.1, 1, 10, and 100 μM concentrations of methotrexate, methotrexate-(G3)PAMAM conjugate, and the vehicle DMSO. LLC cell proliferation is monitored by counting the number of cells in each well

at the 24, 36, 48, 60, and 72 hour time points, using a MTT assay. The data is collected and cross-compared in order to determine the biological effect of the methotrexate-PAMAM(3G) conjugate on tumor cells in hypoxic and normal media.

3.2. Results

In the assay performed by Dr. Kabir, cell proliferation was monitored and reported as the percentage of cells counted at a given time point relative to initial number of cells (1000 in the protocol described above).

Figure 3.1: At the 24 hour time point, there was little difference in cell proliferation among normal LLC cells treated with DMSO, methotrexate, and the methotrexate-(G3)PAMAM conjugate. However, with hypoxic LLC cells, both methotrexate and the methotrexate conjugate had an inhibitory effect on cell proliferation relative to the vehicle. The effect of free methotrexate was the strongest, though the relative inhibitory effect of both disappeared at higher concentrations, indicating that, at high concentrations, the inhibitory effect was dominated by DMSO.

Figure 3.2: At the 36 hour time point, free methotrexate showed a significant inhibitory effect on normal LLC cell proliferation relative to the vehicle DMSO. The effect was not observed with the methotrexate conjugate except at high (100 μM) concentration. With hypoxic cells, however, both free and conjugated methotrexate had an inhibitory effect on cell proliferation. The effect was consistently stronger with free

methotrexate, across all tested non-zero concentrations.

Figure 3.3: At the 48 hour time point, free methotrexate again showed a significant inhibitory effect on normal LLC cell proliferation relative to the vehicle DMSO. However, the effect was not clear at concentrations lower than 0.1 μM. Beyond 0.1 μM, the inhibitory effect of free methotrexate on cell proliferation was stronger with increasing concentration. The methotrexate conjugate also inhibited cell proliferation relative to DMSO, and it did so at concentrations of 10 and 100 μM (the inhibition was slightly stronger at 100 μM). With hypoxic cells, free methotrexate clearly had an inhibitory effect on cell proliferation that was stronger at higher methotrexate concentrations. The methotrexate-(G3)PAMAM conjugate did not show an inhibitory effect relative to DMSO until a concentration of 1 μM. The effect was then increasingly strong with 10 and 100 μM concentrations of the conjugate.

Figure 3.4: At the 60 hour time point, free methotrexate showed a significant inhibitory effect on normal LLC cell proliferation relative to the vehicle DMSO. The effect was clear at concentrations greater than 0.001 μM, and the inhibitory effect of free methotrexate on cell proliferation was stronger with increasing concentration. The methotrexate conjugate again inhibited cell proliferation relative to DMSO, and it did so significantly at concentrations of 10 and 100 μM (the effect was similar in magnitude). With hypoxic cells, free methotrexate had an inhibitory effect on cell proliferation that was stronger at higher methotrexate concentrations, but leveled out after 1 μM. Again, the methotrexate conjugate did not show an inhibitory effect relative to the vehicle until a concentration of 1 μM; beyond 1 μM, the effect was stronger with increasing

concentration.

Figure 3.5: At the 72 hour time point, free methotrexate showed a significant inhibitory effect on normal LLC cell proliferation relative to DMSO. The effect was clear at all concentrations, and was stronger with increasing concentration; however, it leveled off after 1 μM. The methotrexate conjugate again inhibited cell proliferation relative to DMSO, and it did so at all conjugate. As expected, the effect was stronger with increasing concentration. With hypoxic cells, free methotrexate had an inhibitory effect on cell proliferation that was stronger at higher methotrexate concentrations, but again leveled off after treatment concentrations 1 μM. The methotrexate conjugate showed an inhibitory effect relative to the vehicle beyond treatment concentrations of 0.01 μM; again, the effect was stronger with increasing concentrations of the methotrexate conjugate.

Figure 3.6: Taking a cross section of data 10 μM treatment concentrations and following the effect through time, it is clear that the methotrexate conjugate has an inhibitory effect on LLC cell proliferation. The inhibitory effect of the prodrug takes place more slowly than it does with free methotrexate, and the effect is also weaker than that of free drug across all time points.

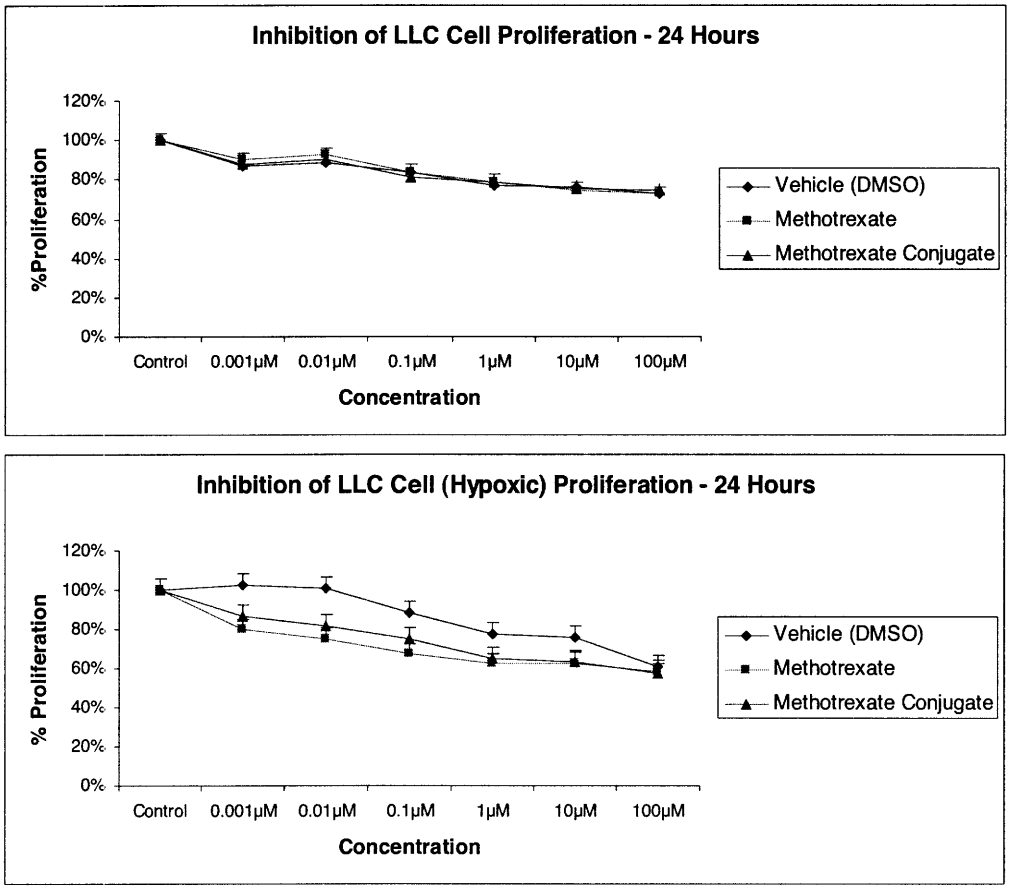

Figure 3.1: Action of methotrexate–(G3)polyamidoamine dendrimer on Lewis Lung Carcinoma cell proliferation *in vitro*. The 24 hour time point shows enhanced inhibition by the conjugate relative to the vehicle and control in a hypoxic environment. As desired, the inhibition effect from the conjugate is slowed and attenuated relative to free methotrexate. Data obtained from experiments designed and performed by Dr. Sujan R. Kabir; used with permission.

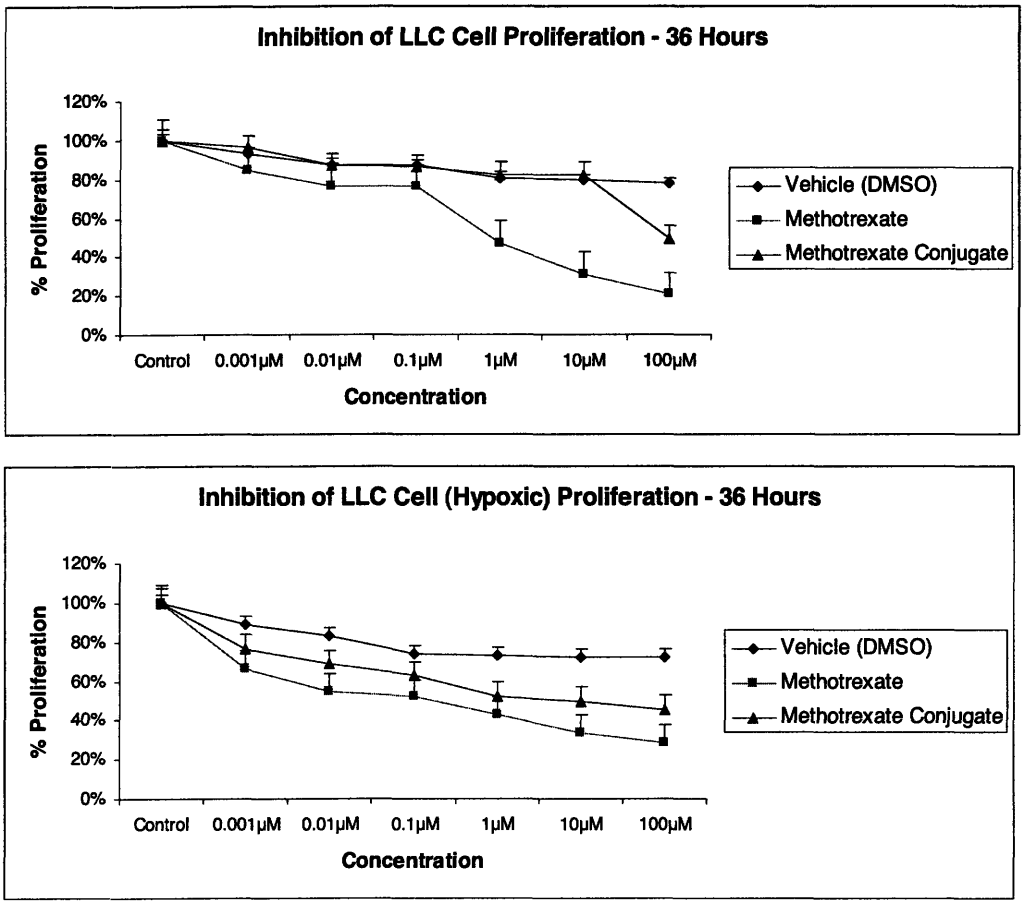

Figure 3.2: Action of methotrexate–(G3)polyamidoamine dendrimer on Lewis Lung Carcinoma cell proliferation *in vitro*. The 36 hour time point also shows significant inhibition by the conjugate relative to the vehicle and control. Similar effects as described in Figure 3.1 are observed, albeit augmented. Data obtained from experiments designed and performed by Dr. Sujan R. Kabir; used with permission.

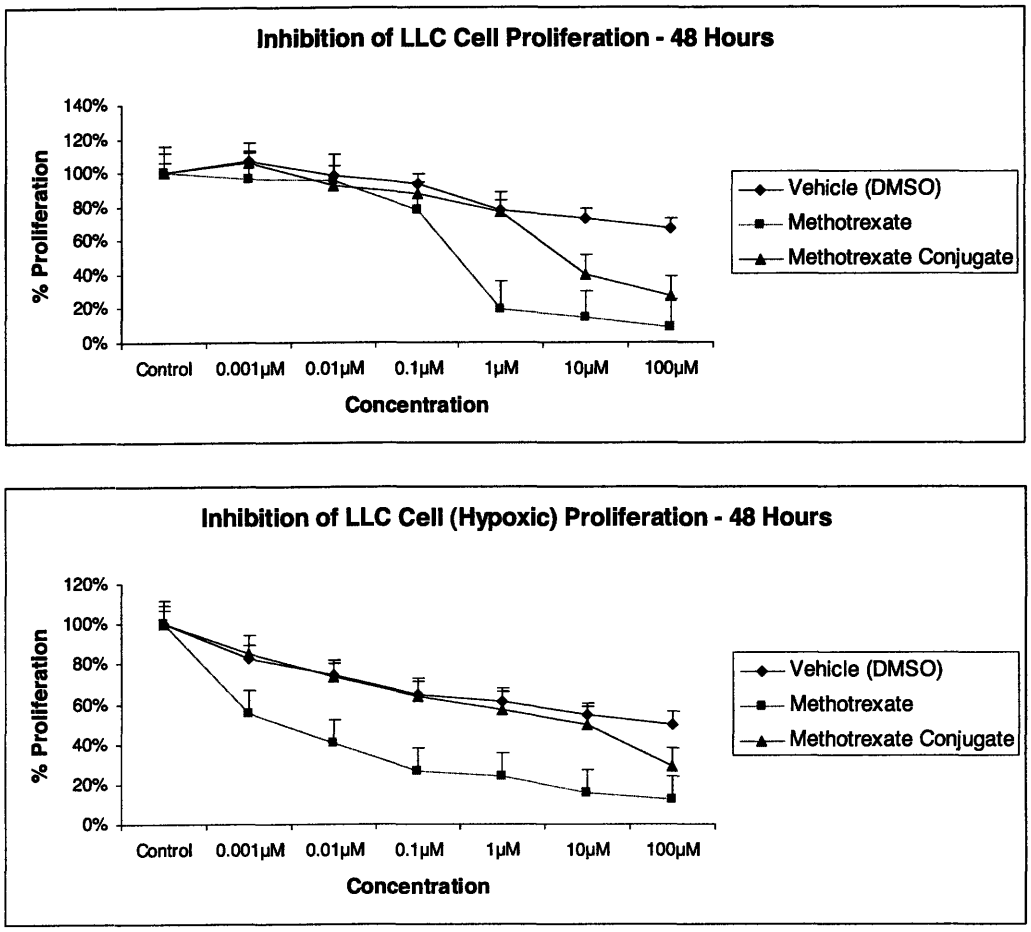

Figure 3.3: Action of methotrexate–(G3)polyamidoamine dendrimer on Lewis Lung Carcinoma cell proliferation *in vitro*, after 48 hours of treatment. Similar effects as described in Figures 3.1 and 3.2 are observed, though the effect of the vehicle DMSO begins to take stronger effect. Data obtained from experiments designed and performed by Dr. Sujan R. Kabir; used with permission.

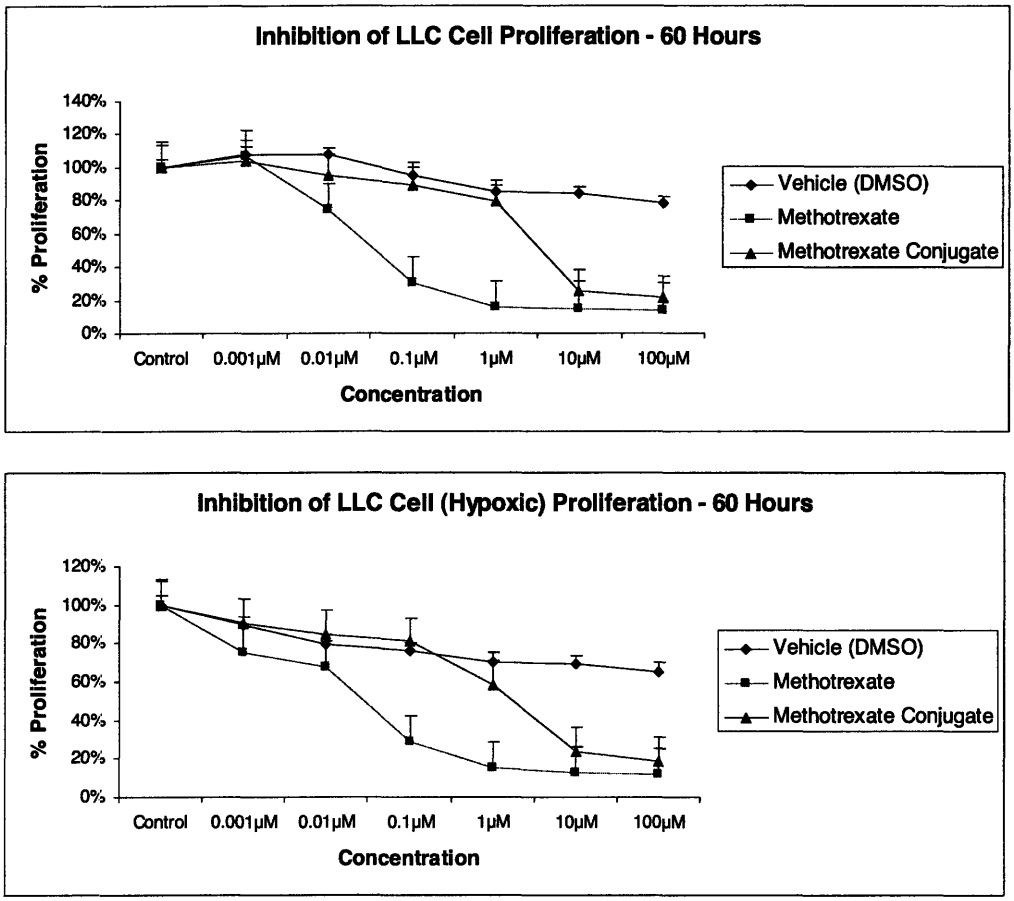

Figure 3.4: Action of methotrexate–(3G)polyamidoamine dendrimer on Lewis Lung Carcinoma cell proliferation *in vitro*. The 60 hour time point also reveals an inhibitory effect on LLC cell proliferation by the conjugate, relative to the vehicle and control. Again, the inhibitory effect of the conjugate is slowed and attenuated relative to free methotrexate. Compared to Figure 3.2, one can see quite clearly the slow-release effects of the methtrexate–(G3)polyamidoamine conjugate. Data obtained from experiments designed and performed by Dr. Sujan R. Kabir; used with permission.

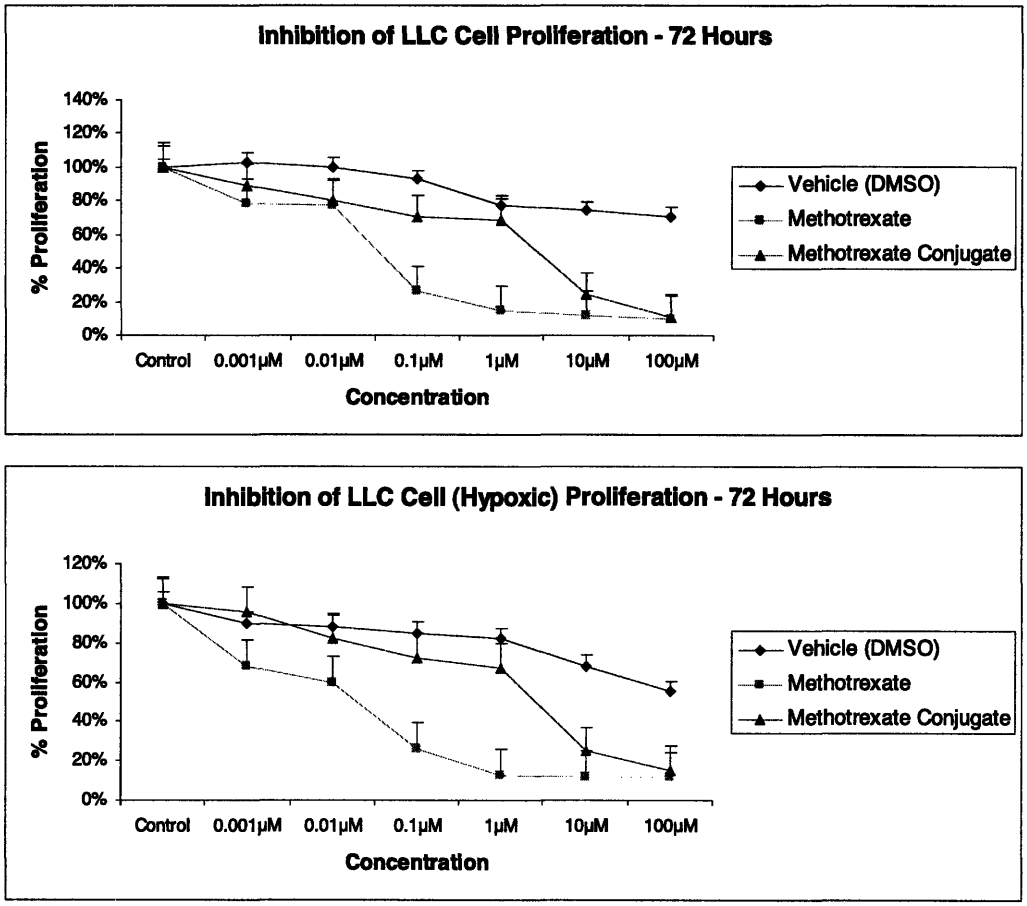

Figure 3.5: Action of methotrexate-(G3)polyamidoamine dendrimer on Lewis Lung Carcinoma cell proliferation in vitro at the final, 72 hour time point. Data obtained from experiments designed and performed by Dr. Sujan R. Kabir; used with permission.

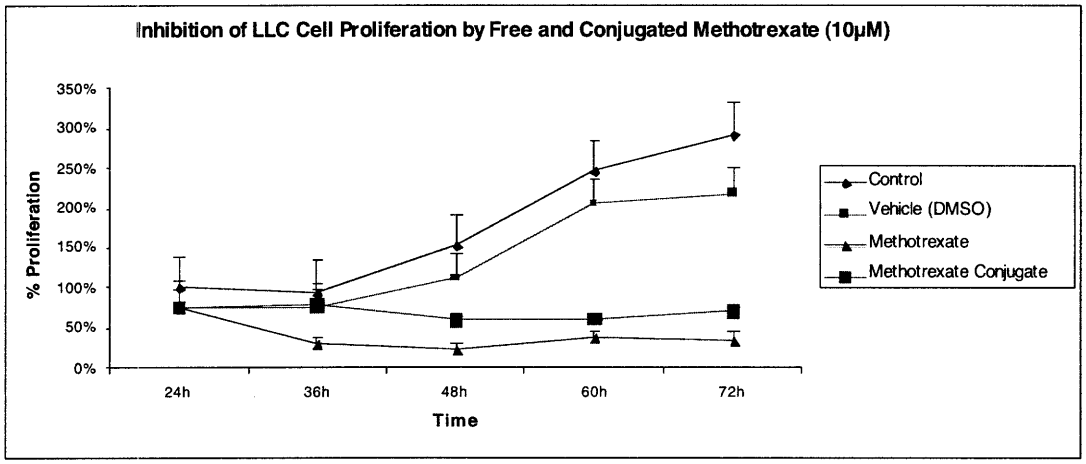

Figure 3.6: Action of methotrexate–(G3)polyamidoamine dendrimer on Lewis Lung Carcinoma cell proliferation *in vitro*. Here, the data is displayed across time, for treatment concentrations of 10 μm. The methotrexate conjugate has an attenuated, inhibitory effect on cell proliferation. Furthermore, in comparing the effect of the conjugate to that of the vehicle, it is evident that the methotrexate–(G3)polyamidoamine conjugate displays slow–release characteristics *in vitro*. Data obtained from experiments designed and performed by Dr. Sujan R. Kabir; used with permission.

3.3 Conclusions and Future Experiments

The cell studies of the methotrexate-(G3)PAMAM conjugate show promising results. First of all, the conjugate maintains bioactivity – methotrexate from the conjugate inhibits LLC cell proliferation relative to the vehicle DMSO across all time-points. The inhibitory effect is, as expected, slower than that of free methotrexate.

The cell studies also reveal that the methotrexate-dendrimer conjugate behaves slightly differently in hypoxic and non-hypoxic environments. From the data presented above, it can be seen that the cytotoxic effect of the conjugate is accelerated in hypoxic environments; the cell studies at the 36-hour time point show this behavior most clearly. However, the effect is diminished at later time points.

In considering these studies, it is important to note that the vehicle, DMSO, has a significant inhibitory effect on LLC cell proliferation (for example, see figure 3.6). The effect of the vehicle may obscure important behavior of the methotrexate-conjugate. Though the cell studies were performed with the vehicle alone for a comparative analysis, it will be important to determine the action of the conjugate in the absence of DMSO. To overcome solubility problems, a slow release, encapsulating particle will be used in future studies.

It should also be determined if the action of the methotrexate-(G3)PAMAM conjugate is the result of esterase-mediated cleavage of methotrexate from the dendrimer. An experiment that eliminates ester hydrolysis via others mechanism would aid in our understanding of the true effect of the nanocell. In order to corroborate the argument that the methotrexate-(G3)PAMAM conjugate selectively releases methotrexate in hypoxic

cellular microenvironments, it would need to be shown that the upregulation of the cleavage mechanism is indeed a result of hypoxia. Furthermore, a conclusive control experiment demonstrating that the conjugate is not bioactive before cleavage should be performed. Recent research has shown that covalent methotrexate-dendrimer conjugates do have cytotoxic effects [Patri et al., 2005].

Keeping the future experiments in mind, these cell studies show that the methotrexate-(G3)PAMAM conjugate is promising candidate for a novel loading mechanism in a nanocell-based approach to cancer therapy. The nuclear magnetic resonance, ultraviolet light absorbance, and transmission electron microscopy studies presented in chapter two, combined with Dr. Kabir's cell studies here, show that the conjugate is an efficient, slow-release drug delivery vehicle that is preferentially bioactive in hypoxic cellular microenvironments. Furthermore, the conjugate is highly consistent in its size and methotrexate carrying capacity.

Bibliography

Patri AK, Kukowska-Latallo JF, Baker JR Jr. Targeted drug delivery with dendrimers: Comparison of the release kinetics of covalently conjugated drug and non-covalent drug inclusion complex. *Adv Drug Deliv Rev.* **57**:2203-2214 (2005).

Chapter 4

Concluding Remarks

In the drive to develop effective cancer therapeutics, the nanocell is a very promising concept. It is capable of both spatial and temporal tumor targeting, and thus it can overcome several of the challenges faced by currently available cancer therapeutics. First, relative to current intravenous administration of free drug, the nanocell isolates to tumors and delivers only a minimal amount of drug to other parts of the body. In doing so, the nanocell avoids many of the side effects of current chemotherapy. Second, the temporally controllable release of the two drugs allows the nanocell to accumulate in the tumor, attack the tumor vasculature, and then release chemotherapy drugs within the tumor. Normally, anti-angiogenesis drugs must be administered for several days prior to chemotherapy. Because the chemotherapy drug is delivered to the intratumoral space during anti-angiogenesis therapy rather than after it, higher concentrations and pervasive intratumoral release of the cytotoxic chemotherapy drug can be achieved despite the diminished tumor vasculature. The higher intratumoral concentrations of chemotherapy drug help overcome the HIF-1α mediated stress responses described in chapter one.

4.1 Accomplishments

In improving the nanocell to accommodate the demands of modern medicine, several steps have been taken. First, folate receptor targeting was incorporated into the nanocell envelope. Adding a receptor-targeting layer to the nanocell should allow it target tumor cells with higher specificity than selective extravasation alone. Furthermore, though the experiments were performed using folic acid as the targeting ligand, any ligand may used with the nanocell; the crosslinking required is simply a matter of chemistry. More importantly, an additional tumor-targeting layer – one can be adjusted depending on the type of tumor being treated – has been added to the nanocell.

The second task undertaken was to develop a new loading mechanism for the nanocell. With the general goal of making the nanocell industry viable, and therefore very consistent and efficient, a dendrimer-based loading mechanism was chosen. Dendrimers offer multiple ligand binding sites, as well as a very symmetric structure that is controllable during synthesis. The dendrimer used in this thesis was a third generation polyamidoamine dendrimer with thirty-two ligand-binding sites. The cytotoxic drug methotrexate was conjugated to the dendrimer via the reaction route described in Figure 2.8, and the conjugation efficiency was approximately 70% (Figure 2.9).

Cell studies on the dendrimer demonstrated that it was indeed a bioactive conjugate. The studies showed that the dendrimer exhibits a delayed inhibitory effect on Lewis Lung Carcinoma cell proliferation, as desired. Furthermore, the inhibitory effect is enhanced in hypoxic cellular microenvironments, implying that an additional layer if tumor targeting may be successfully incorporated into future constructions of the

nanocell.

Other work done throughout this thesis project served to demonstrate the expandability of the nanocell concept. A vital aspect of the nanocell is that it is simply an overarching design, a framework for delivering therapeutics to tumors. Because tumors are highly variable, and especially so in the cell-surface receptors they over express and the drugs that they are sensitive to, the nanocell must accommodate many different anti-cancer drugs. The design of the nanocell, however, should consistently allow for the improved delivery of any anti-cancer combination therapy, regardless of the anti-angiogenesis or cytotoxic drugs used. As such, steps were taken towards constructing the nanocell with different cytotoxic drugs.

Future work that will be done includes synthesizing the nanocell and testing it *in vivo*. Such tests were performed with the first-generation nanocell, and naturally, they must be performed with the second-generation nanocell as well. Only *in vivo* tests will reveal the true effectiveness of the tumor targeting mechanisms designed into the second-generation nanocell.

4.2 The nanocell and other particle-based drug delivery vehicles

Much work has been done regarding the delivery of anti-cancer drugs to tumor microenvironments. Several studies have focused on the use of nanoparticles [Brannon-Peppas et al., 2004], liposomes [Sharma et al., 2006], functionalized micelles [Sutton et al., 2007], and more [Reddy 2005] to deliver drugs to tumors. The impetus to use such nanoscale delivery vehicles arises primarily from two sources: the enhanced permeability and retention (EPR) effect of tumor microenvironments [Maeda et al., 2000], and the ability to direct such vehicles to tumor cells using receptor-targeted ligands. Most contemporary approaches to nanoparticle-based drug delivery deliberately take advantage of one of these two motivating factors. The nanocell is unique in that it takes advantage of both. Furthermore, the nanocell is designed to allow for a bolstered EPR effect, as it is may be administered to the patient – without cytotoxic effect – while vascular normalization takes place.

Thus, the nanocell represents a unique and forward-looking approach to tumor targeted drug delivery. The nanocell's design incorporates a broad range of our current understanding of cancer. From the unique cell biology of tumors to the important fluid mechanical properties that such biology inevitably gives rise to, the nanocell takes elements that may be seen as tumor-protective, and uses them to add layers of tumor-targeting to the delivery and release of anti-cancer drugs. As research continues, the ultimate vision is that the nanocell will allow for the synergistic combination of inexpensive chemotherapy and anti-angiogenesis therapy, all while reducing the side effects currently associated with such therapy.

Bibliography

Brannon-Peppas L, Blanchette JO. Nanoparticle and targeted systems for cancer therapy. *Adv Drug Deliv Rev.* **56**(11):1649-1659 (2004).

Maeda H, Wu J, Sawa T, Matsumara Y, Hori K. Tumor vascular permeability and the EPR effect in macromolecular therapeutics: a review. *J Control Release.* 65(1-2):271-284 (2000).

Reddy LH. Drug delivery to tumours: recent strategies. *J Pharm Pharmacol.* **57**(10):1231-1242 (2005).

Sharma G, Anabousi S, Ehrhardt C, Ravi Kumar MN. Liposomes as targeted drug delivery systems in the treatment of breast cancer. *J Drug Target.* **12**(5):301-310 (2006).

Sutton D, Nasongkla N, Blanco E, Gao J. Functionalized micelar systems for cancer targeted drug delivery. *Pharm Res.* E-pub online: 1583-904X (2007).